Manuscript prepared for Geosci. Model Dev.
with version 2014/07/29 7.12 Copernicus papers of the LaTeX class copernicus.cls.
Date: 18 August 2015

A multi-layer land surface energy budget model for implicit coupling with global atmospheric simulations

James Ryder[1], Jan Polcher[2], Philippe Peylin[1], Catherine Ottlé[1], Yiying Chen[1], Eva van Gorsel[3], Vanessa Haverd[3], Matthew J. McGrath[1], Kim Naudts[1], Juliane Otto[1,4], Aude Valade[1], and Sebastiaan Luyssaert[1]

[1]Laboratoire des Sciences du Climat et de l'Environnement (LSCE-IPSL, CEA-CNRS-UVSQ), Orme des Merisiers, 91191 Gif-sur-Yvette, France
[2]Laboratoire de Météorologie Dynamique (LMD, CNRS), Ecole Polytechnique, 91128 Palaiseau, France
[3]CSIRO Oceans & Atmosphere Flagship, 2 Wilf Crane Cr., Yarralumla, ACT 2600, Australia
[4]now at: Climate Service Center 2.0, Helmholtz-Zentrum Geesthacht, Hamburg, Germany

Correspondence to: James Ryder (jryder@lsce.ipsl.fr)

Abstract. In Earth system modelling, a description of the energy budget of the vegetated surface layer is fundamental as it determines the meteorological conditions in the planetary boundary layer and as such contributes to the atmospheric conditions and its circulation. The energy budget in most Earth system models has been based on a 'big-leaf approach', with averaging schemes that represent in-canopy processes. Furthermore, to be stable, that is to say, over large time steps and without large iterations, a surface layer model should be capable of implicit coupling to the atmospheric model. Such models have difficulties in reproducing consistently the energy balance in field observations. We here outline a newly developed numerical model for energy budget simulation, as a component of the land surface model ORCHIDEE-CAN (Organising Carbon and Hydrology In Dynamic Ecosystems - CANopy). This new model implements techniques from single-site canopy models in a practical way. It includes representation of in-canopy transport, a multilayer longwave radiation budget, height-specific calculation of aerodynamic and stomatal conductance, and interaction with the bare soil flux within the canopy space. Significantly, it avoids iterations over the height of the canopy and so maintains implicit coupling to the atmospheric model LMDz (Laboratoire de Météorologie Dynamique Zoomed model). As a first test, the model is evaluated against data from both an intensive measurement campaign and longer term eddy covariance measurements for the intensively studied Eucalyptus stand at Tumbarumba, Australia. The model performs well in replicating both diurnal and annual cycles of energy and water fluxes, as well as the vertical gradients of temperature and of sensible heat fluxes.

1 Introduction

Earth system models are the most advanced tools to predict future climate (Bonan, 2008). These models represent the interactions between the atmosphere and the surface beneath, with the surface formalized as a combination of open oceans, sea-ice and land. For land, a description of the energy budget of the vegetated surface layer is fundamental as it determines the meteorological conditions in the planetary boundary layer and as such contributes to the atmospheric conditions and its circulation.

The vegetated surface layer of the Earth is subject to incoming and outgoing fluxes of energy, namely atmospheric sensible heat (H, Wm^{-2}), latent heat (λE, Wm^{-2}), shortwave radiation from the sun (R_{SW}, Wm^{-2}), longwave radiation (R_{LW}, Wm^{-2}) emitted from other radiative sources such as clouds and atmospheric compounds and soil heat exchange with the subsurface (J_{soil}, Wm^{-2}). The sum of these fluxes is equal to the amount of energy that is stored or released from the surface layer over a given time period Δt (s). So, for a surface of overall heat capacity C_p ($JK^{-1}m^{-2}$) the temperature change over time, ΔT, is described as:

$$C_p \frac{\Delta T}{\Delta t} = R_{LW} + R_{SW} - H - \lambda E + J_{soil} \quad (1)$$

The sign convention used here makes all upward fluxes positive (so a positive sensible or latent heat flux from the surface cools the ground). Likewise a positive radiation flux towards the surface warms the ground.

One key concept in modelling the energy budget of the surface Eq. (1) is the way in which the surface layer is defined. In many cases the surface layer describes both the soil cover and the vegetation above it as a uniform block. Such an approach is known as a 'big leaf model', so called because the entirety of the volume of the trees or crops and the understorey, as well as the surface layer, are simulated in one entity, to produce fluxes parameterised from field measurements. In the model under study, named ORCHIDEE-CAN (Organising Carbon and Hydrology In Dynamic Ecosystems - CANopy) (Naudts et al., 2014), the land surface is effectively simulated as an 'infinitesimal surface layer' - a conceptual construct of zero thickness. As demonstrated in the original paper describing this model, such an approach, whilst reducing the canopy to simple components, was nevertheless able to simulate surface fluxes to an acceptable degree of accuracy for the sites that were evaluated as the original SECHIBA (Schematic of Hydrological Exchange at the Biosphere to Atmosphere Interface) model (Schulz et al., 2001) and later as a component of the original ORCHIDEE model (Krinner et al., 2005), the basis of ORCHIDEE-CAN.

The proof that existing land to surface simulations may now be inadequate comes from intercomparison studies, such as Pitman et al. (2009), which evaluated the response of such models to land use change scenarios. That study found a marked lack of consistency between the models, an observation they attributed to a combination of the varying implementation of LCC (Land Cover Change) maps, the representation of crop phenology, the parameterisation of albedo and the repre-

sentation of evapotranspiration for different land cover types. Regarding the latter two issues, the models they examined did not simulate in a transparent, comparable manner the changes in albedo and evapotranspiration as a result of changes in vegetation cover, such as from forest to cropland. It was not possible to provide a definitive description of the response of latent heat flux to land cover change across the seven models under study, because there was substantial difference in the mechanisms which describe the evaporative response to the net radiation change across the conducted simulations.

Furthermore, the latent and sensible heat fluxes from off-line land surface models were reported to depend very strongly on the process-based parameterisation, even when forced with the same micro-meteorological data (Jiménez et al., 2011).The structure of land surface models, it has been suggested (Schlosser and Gao, 2010), may be more important than the input data in simulating evapotranspiration. Hence, improvements to the soil-surface-atmosphere interaction (Seneviratne et al., 2010), and to the hydrology (Balsamo et al., 2009), are considered essential for better simulating evapotranspiration. We can therefore assert that refinements in the numerical schemes of land surface models represent a logical approach to the further constraint of global energy and water budgets.

Large scale validation, therefore, has revealed that the 'big leaf approach' has difficulties in reproducing fluxes of sensible and latent heat (Jiménez et al., 2011; Pitman et al., 2009; de Noblet-Ducoudré et al., 2012) for a wide range of vegetated surfaces. This lack of modelling capability is thought to be due to the 'big leaf approach' not representing the vertical canopy structures in detail and thus not simulating factors such as radiation partition, separation of height classes, turbulent transport within the vegetation and canopy-atmosphere interactions - all of which are crucial factors in the improved determination of sensible and latent heat flux estimates (Baldocchi and Wilson, 2001; Ogée et al., 2003; Bonan et al., 2014), as well as the presence of an understorey, or mixed canopies, as is proposed by Dolman (1993). Furthermore, a model that is able to determine the temperatures of elements throughout the canopy profile will provide for a more useful comparison with remote sensing devices, for which the 'remotely sensed surface temperature' also depends on the viewing angle. (Zhao and Qualls, 2005, 2006)

This gap in modelling capability provides the motivation for developing and testing a new, multi-layer, version of the energy budget simulation based on Eq. (1). A multi-layer approach is expected to model more subtle but important differences in the energy budget in relation to multi-layer vegetation types such as forests, grasses and crops. Through the simulation of more than one canopy layer, the model could simulate the energy budget of different plant types in two or more layers such as found in savannah, grassland, wood species and agro-forestry systems (Verhoef and Allen, 2000; Saux-Picart et al., 2009)

Where stand-alone surface models have few computational constraints, the typical applications of an Earth System Model (ESM) require global simulations at a spatial resolution of 2°x2° or a higher spatial resolution for century long time scales. Such applications come with a high computational

demand that must be provided for by using a numerical scheme that can run stably over longer time steps (∼15 to 30 minutes), and that can solve a coupled or interdependent set of equations without iterations. In numerics, such a scheme is known as an implicit solution, and requires that all equations in the coupled systems are linearised. Given that ORCHIDEE is the land surface model of the IPSL (Institute Pierre Simon Laplace) ESM, the newly developed multi-layer model was specifically designed in a numerically implicit way.

2 Model requirements

Several alternative approaches to the big leaf model have been developed. These alternatives share the search for a more detailed representation of some of the interactions between the heat and radiation fluxes and the surface layer. Following Baldocchi and Wilson (2001), the range and evolution of such models includes:

1. the big-leaf model (e.g. Penman and Schofield (1951))
2. the big-leaf with dual sources (e.g. Shuttleworth and Wallace (1985))
3. two layer models which split the canopy from the soil layer (e.g. Dolman (1993); Verhoef and Allen (2000); Yamazaki et al. (1992))
4. three layer models, which split the canopy from the soil layer, and simulate the canopy as a seperate understorey and overstorey (e.g. Saux-Picart et al. (2009))
5. one-dimensional multi-layer models (e.g. Baldocchi and Wilson (2001))
6. three-dimensional models that consist of an array of plants and canopy elements (e.g. Sinoquet et al. (2001))

For coupling to an atmospheric model (see below), and thus running at a global scale, simplicity, robustness, generality and computational speed need to be balanced. We therefore propose a one-dimensional multi-layer model combined with a detailed description of the three-dimensional canopy characteristics. We aim for a multi-layer canopy model that:

- simulates processes that are sufficiently well understood at a canopy level such that they can be parameterised at the global scale through (semi-)mechanistic, rather than empirical, techniques. Examples of such processes are the description of stomatal conductance (Ball et al., 1987; Medlyn et al., 2011), and the partition of radiation in transmitted, reflected and absorbed radiation at different canopy levels (Pinty et al., 2006; McGrath et al., in prep.)
- simulates the exposure of each section of the canopy, and the soil layer, to both shortwave and longwave radiation. At the same time the model should also simulate in-canopy gradients, separating between soil-surface - atmosphere and vegetation - atmosphere interactions

- simulates non-standard canopy set-ups, for instance combining different species in the same vertical structure, e.g. herbaceous structures under trees, as explored by Dolman (1993); Verhoef and Allen (2000); Saux-Picart et al. (2009)
- describes directly the interaction between the soil surface and the sub-canopy using an assigned soil resistance rather than a soil-canopy amalgamation
- is flexible, that is to say sufficiently stable to be run over fifty layers or over just two, i.e. the soil-surface and the canopy
- avoids introducing numerics that would require iterative solutions.

Where the first five requirements relate to the process description of the multi-layer model, the last requirement is imposed by the need to couple ORCHIDEE to an atmospheric model. Generally, coupling an implicit scheme will be more stable than an explicit scheme, which means that it can be run over longer timesteps. Furthermore, the approach is robust: for example, if there is an instability in the land surface model, it will tend to be dampened in subsequent timesteps, rather than diverge progressively. For this work, the model needs to be designed to be run over time steps as long as 30 minutes in order to match the timesteps of the IPSL atmospheric model LMDz, to which it is coupled, and so to conserve processing time. However, the mathematics of an implicit scheme have to be linearised and is thus by necessity rigidly and carefully designed. As discussed in Polcher et al. (1998) and subsequently in Best et al. (2004), the use of implicit coupling was widespread in models when the land surface was a simple bucket model, but as the land surface schemes have increased in complexity, explicit schemes have, for most models, been used instead, because complex explicit schemes are more straightforward to derive than implicit schemes. As they demonstrate, there is nevertheless a framework for simulating all land-surface fluxes and processes (up to a height of, say, 50 m, so including above canopy physics) in a tiled 'non-bucket' surface model coupled, using an implicit scheme, to an atmospheric model.

3 Model description

We here summarise the key components of the new implicit multi-layer energy budget model. The important innovation, compared to existing multi-layer canopy models that work at the local scale (e.g. Baldocchi (1988); Ogée et al. (2003)), is that we will solve the problems implicitly - i.e. all variables are described in terms of the 'next' timestep. The notation used here is listed in full in Table 1, and is chosen to complement the description of the LMDz coupling scheme, as is described in Polcher et al. (1998). A complete version of the derivation of the numerical scheme is provided in the supplementary material.

We propose to regard the canopy as a network of potentials and resistances, as shown in Figure 1, a variation of which was first proposed in Waggoner et al. (1969). At each level in the network we

have the state variable potentials: the temperature of the atmosphere at that level, the atmospheric humidity and the leaf level temperature. We include in the network fluxes of latent heat and sensible heat between the leaves at each level and the atmosphere, and vertically between each canopy level. The soil surface interacts with the lowest canopy level, and uppermost canopy level interacts with the atmosphere. We also consider the absorption and reflection of radiation by each vegetation layer and by the surface (SW and LW) and emission of radiation (LW only). This represents the 'classic' multi-layer canopy model formulation, with a network of resistances that simulate the connection between the soil surface temperature and humidity, and fluxes passing through the canopy to the atmosphere.

The analogy is the 'circuit diagram' approach, for which T_a and q_a represent the atmospheric 'potentials' of temperature and specific humidity at different heights and H and λE are the sensible and latent heat fluxes that act as 'currents' for these potentials. At each level within the vegetation, T_a and q_a interact with the leaf level temperature and humidity T_L and q_L through the resistances R_i (for resistance to sensible heat flux) and R'_i (for resistance to latent heat flux). The change in leaf level temperature is determined by the energy balance at each level.

The modelling approach formalises the following constraints and assumptions.

3.1 Leaf vapour pressure assumption

We assume that the air within leaf level cavities is completely saturated. This means that the vapour pressure of the leaf can be calculated as the saturated vapour pressure at that leaf temperature (Monteith and Unsworth, 2008). Therefore the change in pressure within the leaf is assumed proportional to the difference in temperature between the present timestep and the next one, multiplied by the rate of change in saturated pressure against temperature.

$$q_0 \equiv q_{leaf,i}^{t+1} = q_{sat}^{T_{leaf,i}^t} + \frac{\partial q_{sat}}{\partial T}|_{T_{leaf,i}^t}(T_{leaf,i}^{t+1} - T_{leaf,i}^t) \quad (2)$$

$$= \frac{\partial q_{sat}}{\partial T}|_{T_{leaf,i}^t}(T_{leaf,i}^{t+1}) + \left(q_{sat}^{T_{leaf,i}^t} - T_{leaf,i}^t \frac{\partial q_{sat}}{\partial T}|_{T_{leaf,i}^t}\right) \quad (3)$$

$$= \alpha_i T_{leaf,i}^{t+1} + \beta_i \quad (4)$$

where α_i and β_i are regarded as constants for each particular level and timestep, so $\alpha_i = \frac{\partial q_{sat}}{\partial T}|_{T_{leaf,i}^t}$ and $\beta_i = \left(q_{sat}^{T_{leaf,i}^t} - T_{leaf,i}^t \frac{\partial q_{sat}}{\partial T}|_{T_{leaf,i}^t}\right)$

To find a solution we still need to find an expression for the terms $q_{sat}^{T_{leaf,i}^t}$ and $\frac{\partial q_{sat}}{\partial T}|_{T_{leaf,i}^t}$ in α_i and β_i above.

Using the empirical approximation of Tetens (e.g., Monteith and Unsworth, 2008, 2.1) and the specific humidity vapour pressure relationship we can describe the saturation vapour pressure to within 1 Pa up to a temperature of about $35\,^\circ\mathrm{C}$. So the specific humidity of the leaf follows a relationship to the leaf temperature that is described by a saturation curve.

3.2 Derivation of the leaf layer resistances (R_i and R'_i)

The variables R_i and R'_i represent, in our circuit diagram analogue, resistances to the sensible and latent heat flux, respectively.

The resistance to the sensible heat flux, that we refer to as R_i, is equal to the boundary layer resistance, $R_{b,i}$, of the leaf surface:

$$R_i = R_{b,i} \tag{5}$$

For sensible heat flux, $R_{b,i}$ is calculated as:

$$R_{b,i} = \frac{d_l}{D_{h,air} \cdot Nu} \tag{6}$$

for which $D_{h,air}$ is the heat diffusivity of air and d_l is the characteristic leaf length.

The Nusselt number, Nu, is calculated as in (Grace & Wilson, 1976) for which:

$$Nu = 0.66 Re^{0.5} Pr^{0.33} \tag{7}$$

where Pr is the Prandtl number (which is 0.70 for air), and Re is the Reynolds number, for which:

$$Re = \frac{d_l u}{\mu} \tag{8}$$

where μ is the kinematic viscosity of air (= $0.15 cm^2 s^{-1}$), d_l is again the characteristic dimension of the leaf and u is the wind speed at the level i in question.

The resistance to latent heat flux is calculated as the sum of the boundary layer resistance (which is calculated slightly differently) and the leaf stomatal resistance:

$$R'_i = R'_{b,i} + R_{s,i} \tag{9}$$

In this case we use the following expression:

$$R_{b,i} = \frac{d_l}{D_{h,H_2O} \cdot Sh} \tag{10}$$

in which D_{h,H_2O} is the heat diffusivity of water vapour and Sh is the Sherwood number, which for laminar flow is:

$$Sh = 0.66 Re^{0.5} Sc^{0.33} \tag{11}$$

and for turbulent flow is:

$$Sh = 0.03 Re^{0.8} Sc^{0.33} \tag{12}$$

for which Sc is the Schmidt number. The transition from laminar to turbulent flow takes place in the model when the Reynolds number exceeds a value of 8000 (Baldocchi, 1988).

The stomatal conductance, $g_{s,i}$ is calculated according to the Ball-Berry approximation, per level i. In summary:

$$g_{s,i} = LAI_i(g_0 + \frac{a_1 A h_s}{C_s}) \tag{13}$$

where g_0 is the residual stomata conductance, A the assimilation rate, h_s the relative humidity at the leaf surface and C_s the concentration of CO_2 at the leaf surface.

This is one of three simultaneous equations for the stomatal conductance, which is tied to the demand and supply of CO_2 in the leaf. The description here is related to that of the standard Orchidee model (e.g., LSCE/IPSL, 2012, 2.1), for which the g_s that is used to determine the energy budget is calculated as an amalgamated value, over the sum of all levels i. However, in this new energy budget description we keep seperate the g_s for each level i, and use the inverse of this conductance value to determine the resistance that is $R_{s,i}$. Furthermore, the amount of water that is supplied to the plant is calculated, both at the soil and leaf level (Naudts et al., 2014). In times of drought, the water supply term may be lower than the theoretical latent flux than can be emitted for a certain g_s, using equation Eq. (29). In these cases, the g_s term at leaf level is restricted to that corresponding to the supply term limited latent heat flux at the level in question.

3.3 Leaf interaction with precipitation

Both soil interactions and leaf level evaporation components are parameterised using the same interception and evaporation coefficients as are used in the existing ORCHIDEE model (Krinner et al. (2005); LSCE/IPSL (2012)), extended by ORCHIDEE-CAN. Notably, ORCHIDEE-CAN assumes horizontal clumping of plant species, and hence canopy gaps, as opposed to the uniform medium that is applied in the original ORCHIDEE. A portion of rainfall is intercepted by the vegetation (i.e. a canopy interception reservoir), as determined by the total canopy LAI and by the PFT, where it will be subject to evaporation as standing water. The rest falls on the soil surface, and is treated in the same way as for bare soil in the existing model.

3.4 The leaf energy balance equation for each layer

For vegetation, we assume the energy balance is satisfied for each layer. We extend Eq. (1) in order to describe a vegetation layer of volume ΔV_i, area ΔA_i and thickness Δh_i:

$$dV_i \theta_i \rho_v \frac{dT_{leaf,i}}{dt} = (R_{SW,i} + R_{LW,i} - H_i + -\lambda E_i)\Delta A_i \tag{14}$$

All terms are defined in Table 1. The specific heat of each vegetation layer (θ_i) is assumed equal to that of water, and is modulated according to the Leaf Area Density (m^2/m^3) at that level. Since the fluxes in the model are described per square metre, ΔA_i may be represented by the Plant Area Density $(PAD, m^2/m^3)$ for that layer, where 'plant' denotes leaves, stems, grasses or any other vegetation included in optical Leaf Area Index (LAI) measurements. Note that LAI, that has units of

m^2/m^2, is a value that describes the integration over the whole of the canopy profile of PAD (which is applied per metre of height, hence the dimension m^2/m^3). Canopy layers that do not contain foliage may be accounted for at a level by assigning that $R_i = R'_i = \infty$ for that level (i.e. an open circuit).

Rewriting Eq. (14) in terms of the state variables and resistances that are shown in Figure 1 means that R_i is the resistance to sensible heat flux and R'_i the resistance to latent heat flux. Dividing both sides of the equation by ΔV_i, the volume of the vegetation layer (equal to Δh_i multiplied by ΔA_i), expresses the sensible and latent heat fluxes between the leaf and the atmosphere as:

$$(a) \quad \boxed{\theta_i \rho_v \frac{dT_{leaf,i}}{dt} = \left(R_{SW,i} + R_{LW(tot),i} - C_p^{air} \rho_a \frac{(T_{leaf,i} - T_{a,i})}{R_i} - \lambda \rho_a \frac{(q_{leaf,i} - q_{a,i})}{R'_i} \right) \left(\frac{1}{\Delta h_i} \right)} \tag{15}$$

n.b. this is the first of three key equations that are labelled (a), (b) or (c) on the left hand side, throughout.

3.5 Vertical transport within a column

The transport equation between each of the vegetation layer segments may be described as:

$$\frac{d(\rho\chi)}{dt} + div(\rho\chi u) = div(\Gamma grad(\chi)) + S_\chi \tag{16}$$

where div is the operator that calculates the divergence of the vector field, χ is the property under question, ρ is the fluid density, u is the horizontal wind speed vector, S_χ is the concentration for the property in question and Γ is a parameter that will in this case be the diffusion coefficient $k(z)$.

To derive from this expression the conservation of scalars equation, as might be applied to vertical air columns, we proceed according to the Finite Volume Method, as used in the FRAME (Fine Resolution Atmospheric Multi-pollutant Exchange; Singles et al. (1998)) model and as outlined in Vieno (2006) and derived from Press (1992). The final equation is specific to a one-dimensional model, and so does not include a term of the influence of horizontal wind. The resulting expression is sufficiently flexible to allow for variation in the height of each layer, but we preserve vegetation layers of equal height here for simplicity:

$$\frac{d\chi}{dt}\Delta V = \frac{d}{dz}\left(k(z) \frac{d\chi}{dz} \right) \Delta A + S(z)\Delta V \tag{17}$$

$$= -\frac{d}{dz}\left(F(z) \right) \Delta A + S(z)\Delta V \tag{18}$$

where F is the vertical flux density, z represents coordinates in the vertical and x coordinates in the streamwise direction. χ may represent the concentration of any constituent that may include water vapour or heat, but also gas or aerosol phase concentration of particular species. S represents the source density of that constituent (in this case the fluxes of latent and sensible heat from the vegetation layer), and the transport $k(z)$ term represents the vertical transport between each layer.

In the equation above, we substitute the flux-gradient relationship according to the expression:

$$F(z) = -k(z)\frac{d\chi}{dz} \tag{19}$$

This approach allows future applications to include a supplementary term to simulate emissions or deposition of gas or aerosol based species using the same technique.

The transport terms, per level i in the vertically discretised form, are calculated using the 1D second-order closure model of Massman and Weil (1999), which makes use of the LAI profile of the stand. Fuller details are outlined in that paper, but the in-canopy windspeed is dependent on C_{Deff}, the effective phytoelement canopy drag coefficient. This is defined according to Wohlfahrt and Cernusca (2002):

$$C_{Deff} = a_1^{-LAD/a_2} + a_3^{-LAD/a_4} + a_5 \tag{20}$$

where LAD is the Leaf Area Density and a_1, a_3 and a_5 are parameters to be defined.

This second-order closure model also provides profiles of σ_w, the standard deviation in vertical velocity and T_L, the Lagrangian timescale within the canopy. The term T_L is defined as in the model of Raupach (1989a) and represents the time, since 'emission' at which an emitted flux transitions from the near field (emitted equally in all directions, and not subject to eddy diffusivity), and the far field (which is subject to normal eddy diffusivity and gradient influences). The eddy diffusivity $k_i(z)$ is then derived in the far-field using the expressions from Raupach (1989b):

$$k_i = \sigma_{w,i}^2 T_{L,i} \tag{21}$$

However, the simulation of near field transport requires ideally a Lagrangian solution (Raupach, 1989a). As that is not directly possible in this implicit solution, we instead adopt a method developed by Makar et al. (1999) (and later Stroud et al. (2005) and Wolfe and Thornton (2010)) for the transport of chemistry species in canopies for which a 'near-field' correction factor R_{nf} is introduced to the far-field solution, which is based on the ratio between the Lagrangian timescale T_L and τ, which represents the time since emission for a theoretical near-field diffusing cloud of a canopy source, as defined in Raupach (1989a) which, unlike for the far-field, acts as point source travelling uniformly in all directions. In fact the expression for R_{nf} depends ultimately on the ratio of T_L and τ, rather than their absolute values. As there is a direct relationship between the ratio τ and R_{nf} (Figure 2 of Makar et al. (1999)), we here tune the model directly with R_{nf}, as a proxy for τ/T_L. R_{nf} appears to depend on canopy structure and on venting (Stroud et al., 2005), but has yet to be adequately described.

There is thus a modified expression for k_i, with R_{nf} acting effectively as a tuning coefficient for the near-field transport:

$$k_i^* = R_{nf}(\tau)\sigma_{w,i}^2 T_{L,i} \tag{22}$$

The necessity to account for the near-field transport effect in canopies, remains a question under discussion (McNaughton and van den Hurk, 1995; Wolfe and Thornton, 2010).

3.5.1 Fluxes of sensible and latent heat between the canopy layers

We re-write the expression for scalar conservation (Eq. (16), above), as applied to canopies, as a pair of expressions for the fluxes of sensible and latent heat (so, comparing with Eq. (16), $\chi \equiv T$ or q, $F \equiv H$ or λE and $S \equiv$ (the source sensible or latent heat flux at each vegetation layer)).

Neither the sensible or latent heat flux profile is constant over the height of the canopy. The rate of change of $T_{a,i}$ (the temperature of the atmosphere surrounding the leaf at level i) and $q_{a,i}$ (the specific humidity of the atmosphere surrounding the leaf at level i) are proportional to the rate of change of the respective fluxes with height and the source of heat fluxes from the leaf at that level:

$$(b) \quad C_p^{air}\rho_a \frac{dT_{a,i}}{dt}\Delta V_i = -\frac{dH_{a,i}}{dz}\Delta V_i + \left(\frac{T_{leaf,i} - T_{a,i}}{R_i}\right)\left(\frac{C_p^{air}\rho_a}{\Delta h_i}\right)\Delta V_i \tag{23}$$

now we assume the flux-gradient relation and so write Eq. (19) according to sensible heat flux at level i, $H_{a,i}$:

$$H_{a,i} = -(\rho_a C_p^{air})k_i^* \frac{dT_{a,i}}{dz} \tag{24}$$

which is substituted in Eq. (23)

$$(b) \quad \boxed{\frac{dT_{a,i}}{dt}\Delta V_i = \frac{d^2(k_i^* T_{a,i})}{dz^2}\Delta V_i + \left(\frac{T_{leaf,i} - T_{a,i}}{R_i}\right)\left(\frac{1}{\Delta h_i}\right)\Delta V_i} \tag{25}$$

and following the same approach for the expression for latent heat flux at level i, $\lambda E_{a,i}$:

$$(\lambda E)_{a,i} = -(\lambda\rho_a)k_i^* \frac{dq_{a,i}}{dz} \tag{26}$$

which is, again, substituted in Eq. (23):

$$(c) \quad \lambda\rho_a \frac{dq_{a,i}}{dt}\Delta V_i = -\frac{d(\lambda E)_{a,i}}{dz}\Delta V_i + \left(\frac{q_{L,i} - q_{a,i}}{R_i'}\right)\left(\frac{\lambda\rho_a}{\Delta h_i}\right)\Delta V_i \tag{27}$$

$$= -\frac{d(\lambda E)_{a,i}}{dz}\Delta V_i + \left(\frac{(\alpha T_{leaf,i} + \beta_i) - q_{a,i}}{R_i'}\right)\left(\frac{\lambda\rho_a}{\Delta h_i}\right)\Delta V_i \tag{28}$$

$$(c) \quad \boxed{\frac{dq_{a,i}}{dt}\Delta V_i = \frac{d^2(k_i^* q_{a,i})}{dz^2}\Delta V_i + \left(\frac{(\alpha T_{leaf,i} + \beta_i) - q_{a,i}}{R_i'}\right)\left(\frac{1}{\Delta h_i}\Delta V_i\right)} \tag{29}$$

We have now defined the three key equations in the model:

- eqn. (a) balances the energy budget at each canopy air level
- eqn. (b) balances heat fluxes vertically between each vegetation level and 'horizontally' between each vegetation level and the surrounding air

– eqn. (c) balances humidity fluxes in the same sense as for eqn. (b)

The equations must be solved simultaneously, whilst at the same time satisfying the constraints of an implicit scheme.

3.5.2 Write equations in implicit format

The difference between explicit and implicit schemes is that an explicit scheme will calculate each value of the variable (i.e. temperature and humidity) at the next time step entirely in terms of values from the present time step. An implicit scheme requires the solution of equations that couple together values at the next time step. The basic differencing scheme for implicit equations is described by Richtmyer and Morton (1967). In that work, they introduce the method with an example equation:

$$u^{t+1} = B(\Delta t, \Delta x, \Delta y) u^t \tag{30}$$

where B denotes a linear finite difference operator, Δt, Δx, Δy are increments in the respective co-ordinates and u^t, u^{t+1} are the solutions at respectively steps 't' and 't+1'

It is therefore assumed that B depends on the size of the increments Δt, Δx, Δy and that, once known, it may be used to derive u^{t+1} from u^t. So if B can be determined we can use this relationship to calculate the next value in the temporal sequence. However, we necessarily need to know the initial value in the sequence (i.e. u_0). This means that it is an 'initial value problem'. Now, the equivalent of Eq. (30), in the context of a column model, such as LMDz, takes the form:

$$X_i = C_i^X + D_i^X X_{i-1} \tag{31}$$

This describes the state variable X (for example temperature) at level i, in relation to the value at level $i-1$. C_i^X and D_i^X are coupling coefficients that are derived in that scheme. In this particular example, the value of W_i at time t is defined in terms of X_{i-1} at the same timestep.

To maintain the implicit coupling between the atmospheric model (i.e. LMDz) and the land surface model (i.e. ORCHIDEE) we need to express the relationships that are outlined above in terms of a linear relationship between the 'present' timestep t and the 'next' timestep $t+1$. We therefore re-write equations (a), (b) and (c) in implicit form (i.e. in terms of the 'next' timestep, which is $t+1$), as explained in the following subsections.

3.5.3 Implicit form of the energy balance equation

We substitute the expressions for leaf level vapour pressure Eq. (4) to the energy balance equation Eq. (15), which we rewrite in implicit form:

$$(a) \quad \theta_i \rho_v \frac{(T_{leaf,i}^{t+1} - T_{leaf,i}^t)}{\Delta t} = \left(\frac{1}{\Delta h_i}\right)\left(-C_p^{air}\rho_a \frac{(T_{leaf,i}^{t+1} - T_{a,i}^{t+1})}{R_i} + -\lambda\rho_a \frac{(\alpha_i T_{leaf,i}^{t+1} + \beta_i - q_{a,i}^{t+1})}{R_i'} + \eta_1 T_{leaf,i}^{t+1} + \eta_2 + \eta_3 R_{SW}^{down}\right) \tag{32}$$

3.5.4 Implicit form of the sensible heat flux equation

We differentiate Eq. (25) according to the finite volume method Eq. (17), and divide by ΔV_i:

$$(b) \quad \frac{T_{a,i}^{t+1} - T_{a,i}^{t}}{\Delta t} = k_i^* \left(\frac{T_{a,i+1}^{t+1} - T_{a,i}^{t+1}}{\Delta z_i \Delta h_i} \right) - k_{i-1}^* \left(\frac{T_{a,i}^{t+1} - T_{a,i-1}^{t+1}}{\Delta z_{i-1} \Delta h_i} \right) + \left(\frac{1}{\Delta h_i} \right) \frac{(T_{leaf,i}^{t+1} - T_{a,i}^{t+1})}{R_i} \quad (33)$$

3.5.5 Implicit form of the latent heat flux equation

We differentiate Eq. (29) according to the finite volume method Eq. (17), and divide by ΔV_i:

$$(c) \quad \frac{q_{a,i}^{t+1} - q_{a,i}^{t}}{\Delta t} = k_i^* \left(\frac{q_{a,i+1}^{t+1} - q_{a,i}^{t+1}}{\Delta z_i \Delta h_i} \right) - k_{i-1}^* \left(\frac{q_{a,i}^{t+1} - q_{a,i-1}^{t+1}}{\Delta z_{i-1} \Delta h_i} \right) + \left(\frac{1}{\Delta h_i} \right) \frac{(\alpha_i T_{leaf,i}^{t+1} + \beta_i - q_{a,i}^{t+1})}{R_i'} \quad (34)$$

3.5.6 Solution by induction

These equations are solved by deducing a solution based on the form of the variables in Eq. (32), Eq. (33) and Eq. (34) above. The coefficients within this solution can then be determined,with respect to the boundary conditions, by substitution. This is 'solution by induction'.

With respect to Eq. (33), we wish to express $T_{a,i}^{t+1}$ in terms of values further down the column, to allow the equation to solved by 'moving up' the column, as in Richtmyer and Morton (1967). There is also an alternative method to solve these equations also derived from that text, which we describe in the supplementary material.

In order to solve by implicit means, we make the assumption (later to be proved by induction) that:

$$i) \quad \boxed{T_{a,i}^{t+1} = A_{T,i} T_{a,i-1}^{t+1} + B_{T,i} + C_{T,i} T_{leaf,i}^{t+1} + D_{T,i} q_{a,i-1}^{t+1}} \quad (35)$$

$$ii) \quad \boxed{q_{a,i}^{t+1} = A_{q,i} q_{a,i-1}^{t+1} + B_{q,i} + C_{q,i} T_{leaf,i}^{t+1} + D_{q,i} T_{a,i-1}^{t+1}} \quad (36)$$

We then also re-write these expressions in terms of the values of the next level:

$$i) \quad \boxed{T_{a,i+1}^{t+1} = A_{T,i+1} T_{a,i}^{t+1} + B_{T,i+1} + C_{T,i+1} T_{leaf,i+1}^{t+1} + D_{T,i+1} q_{a,i}^{t+1}} \quad (37)$$

$$ii) \quad \boxed{q_{a,i+1}^{t+1} = A_{q,i+1} q_{a,i}^{t+1} + B_{q,i+1} + C_{q,i+1} T_{leaf,i+1}^{t+1} + D_{q,i+1} T_{a,i}^{t+1}} \quad (38)$$

where $A_{T,i}$, $B_{T,i}$, $C_{T,i}$, $D_{T,i}$, $A_{q,i}$, $B_{q,i}$, $C_{q,i}$ and $D_{q,i}$ are constants for that particular level and timestep and are, as yet, unknown, but will be derived. We thus substitute Eq. (35) and Eq. (37)

into Eq. (33) to eliminate T_{t+1}. Symmetrically, we substitute Eq. (36) and Eq. (38) into Eq. (34) to eliminate q_{t+1}.

For the vegetation layer, we conduct a similar procedure, in which the leaf level temperature is described as follows (where E_i, F_i and G_i are known assumed constants for the level and timestep in question):

$$iii) \quad \boxed{T_{leaf,i}^{t+1} = E_i q_{a,i-1}^{t+1} + F_i T_{a,i-1}^{t+1} + G_i} \tag{39}$$

Now the coefficients $A_{T,i}$, $B_{T,i}$, $C_{T,i}$, $D_{T,i}$, $A_{q,i}$, $B_{q,i}$, $C_{q,i}$ and $D_{q,i}$ can be described in terms of the coefficients from the level above and the potentials (i.e. T and q) at the previous timestep, which we can in turn determine by means of the boundary conditions. So we have a set of coefficients that may be determined for each time-step, and we have the means to determine T_S (and q_S via the saturation assumption). We thus have a process to calculate the temperature and humidity profiles for each timestep by systematically calculating each of the coefficients from the top of the column (the 'downwards sweep') then calculating the 'initial value' (the surface temperature and humidity) and finally calculating each T_a, q_a and T_{leaf} by working up the column (the 'upwards sweep'). The term $T_{leaf,i}^{t+1}$ can also be described in terms of the variables at the level below by $T_{leaf,i+1}^{t+1}$ using equation iii) and its terms E_i, F_i and G_i.

3.6 The boundary conditions

3.6.1 The upper boundary conditions

In stand-alone simulations, the top level variables $A_{T,n}$, $C_{T,n}$, $D_{T,n}$ and $A_{q,n}$, $C_{q,n}$, $D_{q,n}$, are set to zero and $B_{T,n}$ and $B_{q,n}$ set to the input temperature and specific humidity, respectively, for the relevant time step (as in Best et al. (2004)) In coupled simulations, $A_{T,n}$, $B_{T,n}$ and $B_{q,n}$, $C_{q,n}$ are taken from the respective values at lowest level of the atmospheric model. Table 2 summarises the boundary conditions for both the coupled and un-coupled simulations.

3.6.2 The lower boundary condition

We need to solve the lowest level transport equations separately, using an approach which accounts for the additional effects of radiation emitted, absorbed and reflected from the vegetation layers:

$$T_S^{t+1} = \frac{T_S^t + \frac{\Delta t}{\theta_0}(\eta_{2,S} + \eta_{3,S} R_{SW}^{down} + \xi_1 + \xi_3 - J_{soil})}{(1 - \frac{\Delta t}{\theta_0}(\xi_2 + \xi_4 + \eta_{1,S}))} \tag{40}$$

where $\eta_{1,S}$, $\eta_{2,S}$ and $\eta_{3,S}$ are components of the radiation scheme, and ξ_1, ξ_2, ξ_3 and ξ_4 are components of the surface flux (where $\phi_H = \xi_1 + \xi_2 T_S^{t+1}$ and $\phi_{LE} = \xi_3 + \xi_4 T_S^{t+1}$; refer to section 3.2 of the supplementary material).

The interaction with the soil temperature is by means of the soil flux term J_{soil}. Beneath the soil surface layer, there is a seven layer soil model (Hourdin, 1992) which is unchanged from the standard version of ORCHIDEE.

3.7 Radiation scheme

The radiation approach is the application of the Longwave Radiation Transfer Matrix (LRTM) (Gu, 1988; Gu et al. 1999), as applied in Ogée et al. (2003). This approach seperates the calculation of the radiation distribution completely from the implicit expression. Instead a single source term for the long wave radiation is added at each level. This means that the distribution of radiation is now completely explicit (i.e. makes use of information only from the 'present' and not the 'next' time step. However, an advantage of the approach is that it accounts for a higher order of reflections from adjacent levels that the single order that is assumed in the process above.

The components for longwave radiation are abbreviated as:

$$R_{LW,i} = \eta_{1,i} T_{leaf,i}^{t+1} + \eta_{2,i} \tag{41}$$

The shortwave radiation component is abbreviated as:

$$R_{SW,i} = \eta_{3,i} R_{SW}^{down} \tag{42}$$

where $\eta_{1,i}$, $\eta_{2,i}$ and $\eta_{3,i}$ are components of the radiation scheme. $\eta_{1,i}$ accounts for the components relating to emission and absorption of LW radiation from the vegetation at level i (i.e. the implicit parts of the long wave scheme) and $\eta_{2,i}$ the components relating to radiation from vegetation at all other levels incident on the vegetation at level i (i.e. the non-implicit part of the long wave scheme).

$\eta_{3,i}$ is the component of the SW radiation scheme - it describes the fraction of the total downwelling short wave light that is absorbed at each layer, including over multiple forward- and back-reflections, as simulated by the multilayer albedo scheme (McGrath et al., in prep.). The fraction of original downwelling SW radiation that is ultimately reflected from the surface and from the vegetation cover back to the canopy can then be calculated using this information.

3.8 The longwave radiation scheme

We applied a version of the Longwave Radiation Transfer Scheme of Gu (1988, 1999), with some modifications that are summarised here. The method assumes that scattering coefficients for longwave radiation are very small (of the order of 0.05), and can thus be ignored.

The basics of the scheme can be described by the matrix equation for a canopy of m levels:

$$\begin{pmatrix} \Delta\aleph_{surf} \\ \Delta\aleph_1 \\ . \\ . \\ . \\ \Delta\aleph_m \\ \Delta\aleph_{above} \end{pmatrix} = \begin{pmatrix} \alpha_{0,0}^{LW} & \alpha_{0,1}^{LW} & . & . & . & \alpha_{0,m}^{LW} & \alpha_{0,m+1}^{LW} \\ \alpha_{1,0}^{LW} & \alpha_{1,1}^{LW} & . & . & . & \alpha_{1,m}^{LW} & \alpha_{1,m+1}^{LW} \\ . & . & & & & & . \\ . & . & & & & & . \\ . & . & & & & & . \\ \alpha_{m,0}^{LW} & \alpha_{m,1}^{LW} & . & . & . & \alpha_{m,m}^{LW} & \alpha_{m,m+1}^{LW} \\ \alpha_{m+1,0}^{LW} & \alpha_{m+1,1}^{LW} & . & . & . & \alpha_{m+1,m}^{LW} & \alpha_{m+1,m+1}^{LW} \end{pmatrix} \begin{pmatrix} \sigma(T_{surf}^t)^4 \\ \sigma(T_{leaf,1}^t)^4 \\ . \\ . \\ . \\ \sigma(T_{leaf,m}^t)^4 \\ R_{LW} \end{pmatrix}$$

for which each element $\alpha_{i,j}^{LW}$ is defined as:

$$\alpha_{i,j} = \begin{cases} -1, & \text{i = j = 0.} \\ \Im(\ell_t - \ell_{j-1}) - \Im(\ell_t - \ell_j), & \text{i=0, j=1, 2, ..., m} \\ \Im(\ell_t), & \text{i=0, j=m+1} \\ \Im(\ell_j - \ell_{i-1}) - \Im(\ell_{j-1} - \ell_{i-1}) - \Im(\ell_j - \ell_i) - \Im(\ell_{j-1} - \ell_i), & \text{i=1, 2, ..., m, j=1, 2, ..., i-1} \\ 2\Im(\ell_i) - 2, & \text{i=1, 2, ..., m, j=i} \\ \Im(\ell_i - \ell_{j-1}) - \Im(\ell_i - \ell_j) - \Im(\ell_{i-1} - \ell_{j-1}) - \Im(\ell_{i-1} - \ell_j), & \text{i=1, 2, ..., m, j=i+1, i+2, ..., m} \\ \Im(\ell_t), & \text{i=m+1, j=0} \\ \Im(\ell_j) - \Im(\ell_{j-1}), & \text{i=m+1, j=1, 2, ..., m} \\ -1, & \text{i = m+1, j=m+1.} \end{cases} \tag{43}$$

Now, the column on the left hand side of the expression $\Delta\aleph_i$ represents the net long wave radiation that is absorbed at each level vegetation i, as well as the soil surface layer ($\aleph_{surf}$) and the atmosphere directly above the canopy ($\aleph_{above}$). T_i, is the temperature of each layer, and R_{LW} represents the downwelling long wave radiation from above the canopy.

Here ℓ_i represents the cumulative leaf area index when working up to level i from the ground, that is to say calculated as:

$$\ell_i = \sum_{1}^{i} LAI_i \tag{44}$$

The function $\Im(\ell)$ simulates the effect of canopy structure on the passage of long wave radiation, and is defined as:

$$\Im(\ell) = 2 \int_0^1 e^{-\frac{\ell G_{leaf}(\mu)}{\mu}} \mu d\mu \tag{45}$$

$G_{leaf}(\mu)$ is a function that represents the orientation of the leaves. $\Im(\ell)$ is then solved from integrations.

So multiplying out the terms, we have the an expression for $\Delta\aleph$ at each level:

$$\Delta\aleph = \alpha_{i,0}^{LW}\sigma(T_{surf}^t)^4 + \alpha_{i,1}^{LW}\sigma(T_{leaf,1}^t)^4 ..., ... + \alpha_{i,i}^{LW}\sigma(T_{leaf,i}^t)^4 \\ ..., ... + \alpha i, m^{LW}\sigma(T_{leaf,m}^t)^4 + \alpha_{LW}^{i,m+1} R_{LW} \tag{46}$$

This part of the energy budget model is explicit, relying on temperature at the last time step. However, for the level i in each case we can make the expression semi-implicit, by expressing partly in terms of the leaf temperature at the next time step, through use a truncated Taylor expansion, such that:

$$\alpha_{i,i}^{LW}\sigma(T_{leaf,i}^{t})^4 \approx \alpha_{i,i}^{LW}\sigma(T_{leaf,i}^{t})^4 + 4((T_{leaf,i}^{t})^3(T_{leaf,i}^{t+1}) - T_{leaf,i}^{t}) \quad (47)$$

$$= \alpha_{i,i}^{LW}\sigma(T_{leaf,i}^{t})^3(T_{leaf,i}^{t+1})^4 \quad (48)$$

so, in effect, Eq. (46) can be expressed as:

$$\Delta\aleph = \alpha_{i,0}^{LW}\sigma(T_{surf}^{t})^4 + \alpha_{i,1}^{LW}\sigma(T_{leaf,1}^{t})^4 ..., ... + \alpha_{i,i}^{LW}\sigma(T_{leaf,i}^{t})^3(T_{leaf,i}^{t+1})^4$$
$$..., ... + \alpha i, m^{LW}\sigma(T_{leaf,m}^{t})^4 + \alpha_{LW}^{i,m+1}R_{LW} \quad (49)$$

and so we calculate the matrix (44) above with the central diagonal for which $i = j$ set to zero and designate the coefficients Eq. (41) as:

$$\eta_{1,i} = \alpha_{i,i}^{LW}\sigma(T_{leaf,i}^{t})^3 \quad (50)$$

$$\eta_{2,i} = \aleph_i - 3\alpha_{i,i}^{LW}\sigma(T_{leaf,i}^{t})^4 \quad (51)$$

3.9 The short wave radiation scheme

We implement the scheme from McGrath et al. (in prep.), which is a development of Pinty et al. (2006). The scheme accounts for three-dimensional canopies through use of a domain-averaged structure factor (the effective Leaf Area Index). To summarise, in this approach the SW radiation is divided into several terms at each level expressed as a fraction of the total SW downwelling radiation, as listed below.

Here we use the notation ψ to denote the fraction of the above canopy SW radiation that is absorbed (ψ_i^{abs}), is incoming to each level i either by direct transmission (uncollided) or by reflection (collided) (ψ_i^{in}) or is outgoing from each level i, again by collided (in either direction) or uncollided (downwards) light (ψ_i^{out}).

The symbol '$\downarrow$' refers to the sum of all downwelling shortwave radiation (i.e. directly transmitted radiation, and second order reflected radiation), whilst '$\uparrow$' refers to the sum of all upwelling shortwave radiation (i.e. sum of first-order and second-order reflected radiation from all levels).

- $\psi_{i,\downarrow,out}^{uncollided}$ - uncollided, transmitted albedo that represents light transmitted through level i without striking any element. This is also described as 'unscattered, collimated radiation'.

- $\psi_{i,\downarrow}^{collided}$ - collided, transmitted albedo that represents light transmitted through level i after striking vegetation one or more times. This is also described as 'forward scattered isotropic radiation'.

- $\psi_{i,\uparrow}^{collided}$ - collided, reflected albedo represents light reflected upwards after striking vegetation one or more times. This is also described as 'back scattered isotropic radiation'

Now, using these probabilities of the fate of the light, the equations of Pinty et al. (2006) are applied to each layer of the canopy in turn, initially for the top layer, with the assumption of a black background underneath. Some of the flux is reflected back into the atmosphere, some absorbed, and some transmitted or forward scattered into the level below. The nature of the light (collimated or isotropic) determines how it interacts with the canopy, so these two types of light are accounted for separately in the model. The calculations are repeated for this lower level, with this fraction of the light. Calculations through all of the levels are continued as an iterative process untill all light is accounted for through either reflection (or back scatter) back to the atmosphere or absorption by the vegetation or by the soil.

We use these terms to calculate the light that is absorbed, that is to say everything that is not either transmitted or reflected by the layer, that can be expressed as follows, respectively for the canopy top:

At the top of canopy, level 'n':

$$\psi_{veg,n}^{abs} = 1 + \psi_{n,\uparrow,in}^{cldd} - (\psi_{n,\uparrow,out}^{cldd} + \psi_{n,\downarrow,out}^{(uncldd+cldd)}) \tag{52}$$

An intermediate level 'i':

$$\psi_{i}^{abs} = \psi_{i,\uparrow,in}^{cldd} + \psi_{i,\downarrow,in}^{(uncldd+cldd)} - (\psi_{i,\uparrow,out}^{cldd} + \psi_{i,\downarrow,out}^{(uncldd+cldd)}) \tag{53}$$

At vegetation level 1, where r_{bkg} is the background reflectance, at the surface layer:

$$\psi_{1}^{abs} = (\psi_{1,\downarrow,out}^{(uncldd+cldd)} \cdot r_{bkd}) - (\psi_{1,\uparrow,out}^{cldd} + \psi_{1,\downarrow,out}^{uncldd+cldd}) \tag{54}$$

So we can now say that the total canopy absorption is given by:

$$\psi_{canopy}^{abs} = \sum_{i=1}^{n} \psi_{i}^{abs} \tag{55}$$

and, making use of the above, for the soil surface layer we say:

$$\psi_{surface}^{abs} = 1 - \psi_{canopy}^{abs} - \psi_{n,\uparrow,out}^{cldd} \tag{56}$$

Over the canopy vegetation levels, we can now define the coefficient $\eta_{3,i}$ in equation Eq. (32):

$$\eta_{3,i} = \psi_{i}^{abs} \tag{57}$$

$$\eta_{3,surf} = \psi_{surface}^{abs} \tag{58}$$

4 Model set up and simulations

4.1 Selected site and observations

Given the desired capability of the multi-layer model to simulate complex within canopy interactions, we selected a test site with an open canopy. This is because open canopies may be expected to be more complex in terms of their interactions with the overlying atmosphere. In addition, long-term data measurements of the atmospheric fluxes had to be available in order to validate the performance of the model across years and seasons, and within canopy measurements were required in order to validate the capacity of the model to simulate within canopy fluxes. One site that fullfiled these requirements was the long-term measurement site at Tumbarumba in south-eastern inland Australia ($35.6°$S, $148.2°$E, elevation $\sim$1200m) which is part of the global Fluxnet measurement program (Baldocchi et al., 2001). The measurement site is a *Eucalyptus Delegatensis* canopy, a temperate evergreen species, of tall height $\sim$40m. With an LAI of $\sim$2.4, the canopy is described as 'moderately open'. (Ozflux, 2013)

4.2 Forcing and model comparison data

As a test of stability over a long term run, the model was forced (i.e. run 'off-line', independently from the atmospheric model) using above-canopy measurements. The forcing data that was used in this simulation was derived from the long term Fluxnet measurements for the years 2002 to 2007, specifically above-canopy measurements of longwave and shortwave radiation, temperature, humidity, windspeed, rainfall and snowfall. The first four years of data, from 2002 to 2005, were used as a spin-up to charge the soil to its typical water content for the main simulation. The biomass from the spin-up was overwritten by the observed leaf biomass to impose the observed LAI profile. Soil carbon is not required in this study, which justify the short spin-up time. The years 2006 and 2007 were then used as the main part of the run. Although the shortwave radiation was recorded at the field site in upwelling and downwelling components (using a set of directional radiometers), the long wave radiation was not. As a consequence, the outgoing longwave was calculated using the recorded above canopy temperature with the Stefan-Boltzmann law with an emissivity factor of 0.96 (a standard technique for estimating this variable (e.g. Park et al. (2008)). This value is then subtracted from the net radiation, together with the two shortwave components, to obtain an estimation of the downwelling longwave radiation with which to force the model.

For the validation of the within canopy processes more detailed measurement data were required. For the same site there exists data from an intensive campaign of measurements made during November 2006 (Austral summer), described by Haverd et al. (2009). Within the canopy, profiles of temperature and potential temperature were recorded over the 30 day period and, for a number of days (7^{th}-14^{th} November), sonic anemometers were used to measure windspeed and sensible heat flux in the vertical profile at eight heights as well. Measurements were also made over the thirty day period

of the soil heat flux and the soil water content. These within-canopy data were used for validation of the modelled output but the same above-canopy long-term data (i.e. the Fluxnet data) were used in the forcing file in all cases. No further measurements were collected specifically for this publication. The measurement data (i.e. the data both from the one month intensive campaign and the long term Fluxnet measurements at the same site (Ozflux, 2013)) were prepared as an ORCHIDEE forcing file, according to the criteria for gap-filling missing data (Vuichard and Papale, 2015).

4.3 Model set-up

The multi-layer module that is described in this paper only calculates the energy budget. Its code was therefore integrated in the enhanced model ORCHIDEE-CAN, and relies on that larger model for input-output operations of drivers and simulations, as well as the calculation of soil hydrology, soil heat fluxes and photosynthesis (see Table 3 for other input). A more detailed description of how these processes are implemented in ORCHIDEE-CAN is provided in Naudts et al. (2014).

The ORCHIDEE-CAN model is capable of simulating the canopy vegetation structure prognostically, and these prognostic vegetation stands have now been linked to the multi-layer energy budget profile in the current model. In these tests, a vegetation profile was forced, in order to obtain a simulation as close as possible to the observed conditions. That is to say, the stand height to canopy radius ratios of the trees across several size classes in ORCHIDEE-CAN were forced over the course of the spin-up phase to an approximation of the Tumbarumba LAD profile. The assigned height to radius profiles are provided in Table 4. LAD is an estimate of the sum of the surface area of all leaves growing on a given land area (e.g. per m^2) over a metre of height. I'It is effectively LAI (m^2 per m^2) per canopy levels, and thus has units of m^2 per level of the canopy '. As there were no LAD profiles available for the field site at the time of measurement, data from Lovell et al. (2012) for the 'Tumbatower' profile, as depicted in Figure 3 of that publication, were used as a template. The profile was scaled according to the measured site LAI of 2.4, resulting in the profile shown in Figure 2. As no gap-forming or stand replacement disturbances have been recorded at the site, the vertical distribution of foliage was assumed unchanged over the period between the different measurement campaigns.

Several tuning coefficients were applied to constrain the model, which are listed in Table 4. A combination of manual and automated tuning was used to tune the model as closely as possible to the measurement data. The key tuning coefficients were: $R_{b,fac}$, a tuning coefficient for the leaf boundary layer resistance, $R_{g,fac}$, a coefficient for the stomatal resistance and R_{nf}, the near field correction factor to the modified eddy diffusivity coefficient K_i^*, the coefficients a_1, a_3 and $a_5$corresponding to the definition C_{deff}, from Eq. (20) and Ω, a correction factor for the total LAI to allow for canopy gaps. A fuller guide to the model tuning is provided in (**?**).

5 Results

Although the aim of this study is to check the performance of our multi-layer energy budget model against site-level observations, it should be noted that site-level energy fluxes come with their own limitations that result in a so-called closure gap. The closure gap is reflected in a mismatch between the net radiation and the fluxes of latent, sensible and soil heat. For the observations used in this study, the closure gap was $\sim$37 W/m^2 (7.5% of total fluxes) during the day and 4 W/m^2 (4.6%) during the night. Underestimation of the data and mismatches exceeding the closure gap likely indicate a shortcoming in the model. At a fundamental level, energy budget models distribute the net radiation between sensible, latent and soil heat fluxes. Evaluation of these component fluxes becomes only meaningful when the model reproduces the net radiation (Figure 3). Note that through its dependency on leaf temperature the calculation of the longwave component of net radiation depends on the sensible, latent and soil heat fluxes. Taken as a whole, there is a very good correlation between the observation-driven and model-driven net longwave radiation (r^2 = 0.96). However, when the data are separated into nighttime and daytime, as shown, a clear cycle is revealed, for which the model overestimates daytime radiation and underestimates radiation at night. This discrepancy is likely a result of actual daytime heat storage in the soil being underestimated in the model. A portion of the upwelling longwave radiation is sourced from temperature changes in fluxes from the soil model, and the rest from vegetation. So if the daytime surface layer temperature is underestimated by the model, we expect reduced net longwave predicted radiation, compared to that which is measured, and vice versa for the nighttime scenario. The use of above canopy air temperature, instead of radiative temperature (which was not measured) may also contribute to inaccuracies in the predicted longwave radiation.

In terms of the current parameterisation, and for the site under study, the annual cycles for both sensible and latent heat are well simulated (Figure 4a & 4(c). In addition, no clear systematic bias was observed between summer and winter (Figure 4b & 4(d). But, as shown, there is an overall systematic bias of +12.7W/m^2 for sensible heat and +10.7 W/m^2 for latent heat flux, when averaged over the whole year. Such a bias represents $\sim$23% of sensible heat and $\sim$15% of latent heat fluxes.

The analysis proceeded by further increasing the temporal resolution and testing the capacity of the model to reproduce diurnal flux cycles. The model overestimates the diurnal peak in sensible heat flux, whilst the latent heat flux is underestimated by a smaller magnitude (Figure 5(b)). The diurnal pattern of the model biases persists in all four seasons (Fig Supplementary 1 (a)-(d)). We see that the maximum mean discrepancy between measured and modelled sensible heat flux ranges from + 95W/m^2 to -84 W/m^2 (Figure 5(b)) and latent heat flux from -49 W/m^2 to 43 W/m^2 (Figure 5(d)). Over the course of the year, the difference is largest in the autumn and smallest in the summer (Fig S2 (a)-(d)). However, from the net radiation (i.e. the sum of downwelling minus upwelling for longwave and shortwave), we can see that there is a discrepancy between measured and modelled that acts to offset in part the discrepancy observed in the flux plots (Figure 5(a)-(f)).

Long-term measurements from above the forest and data from a short intensive field campaign were jointly used to evaluate model performance at different levels within the canopy. For reference, Figure S3 summarises the downwelling longwave and shortwave radiation measured over this period. As was the case for the annual cycle, the sinusoidal cycles resulting from the diurnal pattern in solar angle are well matched (Figure 6 (a)-(d)). Sensible heat flux was measured below and above the canopy and the model was able to simulate this gradient (Figure 6(a), (c). Latent heat flux at an equivalent height of 2m was not recorded (Figure 6(d). However, the match in magnitude of the measured data is not accurately simulated hour by hour (Figure 6(e).

Using the current parameters, there is a discrepancy between the measured and the modelled temperature gradients within the canopy (Figure 7). It should be noted that the mean values are strongly determined by a few extreme hours. As such the model is capable of simulating the majority of the time steps but fails to reproduce the more extreme observations. During the daytime, the strong positive gradient in the measured output is only partly reflected in the modelled slopes. At nighttime, there is a clear negative gradient for the measured data, which is matched by the model. These profiles demonstrate that in-canopy gradients can be replicated by paramaterisation of the model.

The version of the model used in these tests so far is composed of 30 levels, with 10 levels in the understorey, 10 in the canopy vegetation profile, and 10 in the overstorey, in order to provide a high resolution simulation and a test of the stability of the scheme. However, a canopy simulation of such detail might be overly complex for a canopy model that is to be coupled to an atmospheric simulation, in terms of additional run time required. To provide an evaluation of the difference in fluxes that were predicted by a model of lower resolution, the same tests were conducted with the model composed of 10, 5, 2 and a single vegetation level, that correspond to a profile that totals 30, 15, 8 and 5 levels over all, when the levels in the overstorey and understorey are included (note that in all cases the vegetation levels are simulated separately from the surface soil level is also treated separately in each case, and represents a separate layer (c.f., Dolman, 1993)).

Tests were conducted for both hourly mean (Figure 8) and daily mean (Figure 9), both calculated over the course of a year, and for a moving average. These plots show the RMS error between the original set up and the a modified number of levels. Looking first at the plots for hourly mean, we see that there is already a significant difference between the calculated sensible heat flux for the version of the model with 10 canopy layers (30 total profile layers) and 5 canopy layers (15 total profile layers), that reaches a peak of 28 W/m^2, but that the discrepancy is substantially larger for the 2 canopy layer (8 total levels) and a single canopy layer (5 total levels) cases. In the case of the latent heat flux, the discrepancy is most marked for the the single canopy layer case, with a peak difference of 60 W/m^2. Considering the daily averages, for sensible heat flux the difference between the different model set-ups is always below 25 W/m^2 in all cases. For latent heat flux, there is more considerable divergence, up to 42 W/m^2, for the single canopy later set-up.

6 Discussion

The proposed model is able to simulate fluxes of sensible and latent heat above the canopy over a long term period, as has been shown by simulation of conditions at a Fluxnet site on a long term, annual scale (Figures 4 and 5), and over a concentrated, week-long period (Figure 6). Although these figures show a discrepancy between measured and modelled fluxes, we see from Figure 5 that the modelled overestimate of sensible heat flux is offset by an underestimation of latent heat flux and of net radiation. In the study of land-atmosphere interactions, the multi-layer model functions to a standard comparable to single-layer models, and an interative model applied to the same site (Haverd et al., 2009) found differences of the order of 50 W/m^2 at maximum for the mean daily average latent and sensible above canopy heat fluxes.

The innovation of this model is the capacity to simulate the behaviour of fluxes within the canopy, and the separation of the soil-level temperature from the temperature of the vegetation levels. Uniquely for a canopy model, this is achieved without iterations, as the mathematics have been derived to use the same implicit coupling technique as the existing surface-atmosphere coupling applied in ORCHIDEE/LMDz (Polcher et al., 1998; Best et al., 2004), but now over the height of the canopy. This also means that the model is scalable without impacting heavily on runtimes. For large scale applications, performance within the canopy must be further constrained through comparison with intensive in-canopy field campaigns from diverse ecosystems.

6.1 Simulation of aerodynamic resistance

In this study, the aerodynamic coefficient that is used in single-layer models was replaced by an eddy diffusivity profile, the purpose of which is two-fold. Firstly, to develop a transport coefficient that is based on the vertical canopy profile and secondly, to more accurately represent the in-canopy gradients of temperature and specific humidity. In this way, it was hoped to contribute to a model that can better allow for such features as vertical canopy gaps (i.e. trunk space between a well separated under and overstorey), horizontal gaps, transport and chemistry between different sections of the canopy, tree growth and the mix of different kinds of vegetation in the same surface layer simulation (e.g. Dolman (1993)). To be able to do this, a height based transport closure model was used to simulate within canopy transport.

The transport closure model used here can be compared to the previous single-layer approach within ORCHIDEE. In that approach, aerodynamic interaction between the land surface and the atmosphere is parametrised by the atmospheric resistance R_a and the architectural resistance R_0. R_a is typically calculated through consideration of the roughness height of the canopy (i.e. small for flat surfaces, large for uneven tall surfaces) which in turn is parameterised in surface layer models by canopy height (e.g., LSCE/IPSL, 2012) (however, LAI can display a better correlation with roughness length (a critical parameter) than it does to canopy height (Beringer et al., 2005)). In

parameterising the roughness length in terms of canopy height alone, no account is made for the clumping of trees, the density of the forest or the phenological changes in stand profile (other than the height) as the stand grows. Some of these changes are compensated for in R_0, the structural coefficient that is unique to each PFT grouping, but does not allow for more subtle effects. To be able to satisfactorily explore such results in a modelling study requires an accurate parametrisation of within-canopy transport.

In this study, canopy transport is parametrised by K-theory, applying the closure model of Massman and Weil (1999) to derive the in-canopy turbulence statistics, based both on the LAI profile and the canopy height. The simulation produces a good estimation of above-canopy fluxes, but the differences between day- and night- time profiles are not well described using the original parametrisation (Figure 7). This means that the model overestimates the nighttime canopy transport, as compared to the daytime simulation.

Looking more broadly, studies of chemical species transport have demonstrated that K-theory, sometimes constrained by a scaling factor, remains a reasonable approximation for above-canopy fluxes, even if the within-canopy gradients are not entirely correct (Gao et al., 1989; Dolman and Wallace, 1991; Makar et al., 1999; Wolfe and Thornton, 2010). The justification for such a scaling factor seems to vary in terms of the form of the canopy structure, likely related to canopy openness (McNaughton and van den Hurk, 1995; Stroud et al., 2005). Here, too, we find that a scaling factor is necessary to match the gradient fluxes though the scaling factor required varies according to the time of day. We now also parameterise the effective phytoelement canopy drag coefficient, C_{Deff}, in order to obtain a more accurate simulation. For a completely satisfactory resolution of this issue, it will be necessary to derive a method to reformulate the method of Raupach (1989a, b) in an implicit form, which lies outside the scope of this paper.

6.2 Simulation of energy partition throughout canopy and soil surface

Trees in a spruce forest have been reported to account for 50% - 60% of the latent heat flux; moisture in the soil itself would have a reduced impact due to soil shading (Baldocchi et al., 2000). Another study found that the fraction of radiation that reaches the soil ranges from 0.05 (forest) to 0.12 (tundra) (Beringer et al., 2005). The same study found that the latent heat flux correlates most closely with the leaf-level vapour pressure deficit - that is to say the difference between the leaf level saturation vapour pressure and the actual vapour pressure of the outside air, rather than between air water vapour pressure and the saturation vapour pressure at the soil level. Since a single layer canopy model regards both the canopy and soil surface as the same entity, the aforementioned subtleties will inevitably be lost in the modelling. Although, the partition of energy between soil surface and vegetation is site dependent - a well hydrated site would behave differently to one in an arid region - it is effects such as these that a more realistic energy budget scheme would be able to simulate.

Being able to simulate separately the vegetation allows for the partitioning of fluxes between the vegetation and the soil. For example, from the measurements (Figure 6 (a) and (b)), we see that approximately 50% of the sensible heat that is measured above the canopy is sourced not from the soil surface, but from the overlying vegetation, as this is the difference between the measured flux at 1m and that above the canopy. The modelling results here overestimate the measured contribution from the soil. There is no equivalent measurement at 1m for the latent heat flux, but the model calculates that approximately 50% of the latent heat flux is sourced from the vegetation rather than the soil surface.

This model also simulates leaf temperature that may be verified by leaf level measurements, where such measurements exist (Helliker and Richter, 2008). Such a comparison would require additional developments (as is discussed in the following section) because leaf temperature measurements strongly depend on the approach that is used.

7 Outlook

This document lays out the framework for the model design, but it allows for the further implementation of many features in site-level to global-scale scenarios:

- As the method calculates leaf temperature and in-canopy radiation, it will be possible to simulate the explicit emission by leaves of certain common Biogenic Volatile Organic Compounds (BVOCs), such as isoprene and monoterpene (Guenther et al., 1995, 2006). As the method calculates in-canopy gradients of temperature, specific humidity and radiation, it is possible to simulate more accurately chemical reactions that depend on these factors such as the NO_x and O_3 cycle within and above canopies (Walton et al., 1997) and the formation and size distribution of aerosol interactions (Atkinson and Arey, 2003; Nemitz et al., 2004a, b; Ehn et al., 2014), which may act as cloud condensation nuclei and thus again feedback into radiation absorption interactions at the atmospheric component of a coupled model such as LMDz/ORCHIDEE.

- Separate computation of vegetation and soil temperatures, which can be very different, and then to estimate accurate estimation of the whole canopy temperature and its directional effects. It may then be possible to assimilate this variable (which can also be measured from remote sensing) in order to better constrain the energy budget.

- Recent research in ecology demonstrates further the need to better understand canopy microclimates, and in particular gradients of state variables such as temperature and specific humidity, and radiation penetration. For example, temperature gradients in the rainforest exert a key influence on the habitat choices of frogs, and changes to such a microclimate threaten their survival (Scheffers et al., 2013). In a similar vein, microclimate affects in canopies can

act as a buffer to changes in the climate overall (i.e. the macro-climate) in terms of the survival of species in the sub-canopy (Defraeye et al., 2014). Therefore structural forest changes, such as forest thinning, will reduce buffer lag effect, but it is only with well-designed canopy models that an informed prediction of the long term consequences of land management policies can be made.

8 Conclusions

A new numerical model for ORCHIDEE-CAN has been developed that enables the simulation of vertical canopy profiles of temperature and moisture using a non-iterative implicit scheme. This means that the new model may also be used when coupled to an atmospheric model, without compromising computer run-time. Initial tests demonstrated that the model runs stably, balances the energy budget at all levels, and provides a good simulation of the measured field data, both on short timescales of a few days, and over the course of a year. As demonstrated, the model structure allows coupling/linking to a more physical-based albedo scheme (Pinty et al., 2006; McGrath et al., in prep.; Naudts et al., 2014) and the implementation of a vertically discretised stomatal conductance scheme. Reducing the vertical discretisation of the canopy from 10 layers to 5, 2 and 1 layer increased the RMSE between the model and the observations for LE and H and thus demonstrates the overall benefits of introducing a multi-layer energy budget scheme. The multi-layer energy budget model component outlined here may be used to simulate canopies in more detail and variety.. It also offers the potential to integrate with other parts of ORCHIDEE for enhanced simulation of CO_2 transport, emission of VOCs and leaf scale plant hydraulics.

9 Author Contributions

JR and JP developed the numerical scheme. YC and JR developed the parameterisation scheme. JR, JP, CO, PP and SL designed the study and JR and SL wrote the manuscript with contributions from all co-authors. YC, MJM, JO, KN, SL and AV helped JR with integrating the multi-layer energy budget model within ORCHIDEE-CAN. EvG and VH provided field observations for the Tumbarumba site.

Acknowledgements. JR, YC, MJM, JO, KN and SL were funded through ERC starting grant 242564 (DOFOCO), and AV was funded through ADEME (BiCaFF). ESA CCI Landcover also supported this work. The study benefited from an STSM (COST, TERRABITES ES0805) offered to JR. We thank the three anonymous reviewers for their very helpful observations and suggestions. The authors would like to thank Aaron Boone for sharing his numerical scheme of an implicit coupling of snowpack and atmosphere temperature. Plots were produced using matplotlib software(Hunter, 2007).

References

Atkinson, R. and Arey, J.: Gas-phase tropospheric chemistry of biogenic volatile organic compounds: a review, Atmospheric Environment, 37, 197–219, doi:10.1016/S1352-2310(03)00391-1, http://linkinghub.elsevier.com/retrieve/pii/S1352231003003911, 2003.

Baldocchi, D. D.: A multi-layer model for estimating sulfur dioxide deposition to a deciduous oak forest canopy, Atmospheric Environment (1967), 22, 869–884, doi:10.1016/0004-6981(88)90264-8, http://linkinghub.elsevier.com/retrieve/pii/0004698188902648, 1988.

Baldocchi, D. D. and Wilson, K.: Modeling CO2 and water vapor exchange of a temperate broadleaved forest across hourly to decadal time scales, Ecological Modelling, 142, 155–184, doi:10.1016/S0304-3800(01)00287-3, http://www.sciencedirect.com/science/article/pii/S0304380001002873, 2001.

Baldocchi, D. D., Law, B. E., and Anthoni, P. M.: On measuring and modeling energy fluxes above the floor of a homogeneous and heterogeneous conifer forest, Agricultural and Forest Meteorology, 102, 187–206, doi:10.1016/S0168-1923(00)00098-8, http://linkinghub.elsevier.com/retrieve/pii/S0168192300000988, 2000.

Baldocchi, D. D., Falge, E., Gu, L., Olson, R., Hollinger, D. Y., Running, S., Anthoni, P., Bernhofer, C., Davis, K., and Evans, R.: FLUXNET: A new tool to study the temporal and spatial variability of ecosystem-scale carbon dioxide, water vapor, and energy flux densities., Bulletin of the American Meteorological Society, 82, 2415–2434, http://ddr.nal.usda.gov/handle/10113/118, 2001.

Ball, J. T., Woodrow, T., and Berry, J.: A model predicting stomatal conductance and its contribution to the control of photosynthesis under different environmental conditions, in: Proceedings of the 7th International Congress on Photosynthesis, pp. 221–224, 1987.

Balsamo, G., Beljaars, A., Scipal, K., Viterbo, P., van den Hurk, B., Hirschi, M., and Betts, A. K.: A revised hydrology for the ECMWF model: verification from field site to terrestrial water storage and impact in the integrated forecast system, Journal of Hydrometeorology, 10, 623–643, doi:10.1175/2008JHM1068.1, http://journals.ametsoc.org/doi/abs/10.1175/2008JHM1068.1, 2009.

Beringer, J., Chapin, F. S., Thompson, C. C., and Mcguire, A. D.: Surface energy exchanges along a tundra-forest transition and feedbacks to climate, Agricultural and Forest Meteorology, 131, 143–161, doi:10.1016/j.agrformet.2005.05.006, 2005.

Best, M. J., Beljaars, A. C. M., Polcher, J., and Viterbo, P.: A proposed structure for coupling tiled surfaces with the planetary boundary layer, Journal of Hydrometeorology, 5, 1271–1278, 2004.

Bonan, G. B.: Forests and climate change: forcings, feedbacks, and the climate benefits of forests, Science, 320, 1444–1449, doi:10.1126/science.1155121, http://www.sciencemag.org/content/320/5882/1444.short, 2008.

Bonan, G. B., Williams, M., Fisher, R. a., and Oleson, K. W.: Modeling stomatal conductance in the earth system: linking leaf water-use efficiency and water transport along the soil–plant–atmosphere continuum, Geoscientific Model Development, 7, 2193–2222, doi:10.5194/gmd-7-2193-2014, http://www.geosci-model-dev.net/7/2193/2014/, 2014.

de Noblet-Ducoudré, N., Boisier, J.-P., Pitman, A., Bonan, G. B., Brovkin, V., Cruz, F., Delire, C., Gayler, V., van den Hurk, B. J. J. M., Lawrence, P. J., van der Molen, M. K., Müller, C., Reick, C. H., Strengers, B. J., and Voldoire, A.: Determining robust impacts of land-use-induced land cover changes on surface climate over North America and Eurasia: Results from the first set of LUCID experiments, Journal

of Climate, 25, 3261–3281, doi:10.1175/JCLI-D-11-00338.1, http://journals.ametsoc.org/doi/abs/10.1175/JCLI-D-11-00338.1, 2012.

Defraeye, T., Derome, D., Verboven, P., Carmeliet, J., and Nicolai, B.: Cross-scale modelling of transpiration from stomata via the leaf boundary layer, Annals of Botany, 114, 711–723, doi:10.1093/aob/mct313, http://www.ncbi.nlm.nih.gov/pubmed/24510217, 2014.

Dolman, A. J.: A multiple-source land surface energy balance model for use in general circulation models, Agricultural and Forest Meteorology, 65, 21–45, doi:10.1016/0168-1923(93)90036-H, http://linkinghub.elsevier.com/retrieve/pii/016819239390036H, 1993.

Dolman, A. J. and Wallace, J.: Lagrangian and K-theory approaches in modelling evaporation from sparse canopies, Quarterly Journal of the Royal Meteorological Society, 117, 1325–1340, http://onlinelibrary.wiley.com/doi/10.1002/qj.49711750210/abstract, 1991.

Ehn, M., Thornton, J. A., Kleist, E., Sipilä, M., Junninen, H., Pullinen, I., Springer, M., Rubach, F., Tillmann, R., Lee, B., Lopez-Hilfiker, F., Andres, S., Acir, I.-H., Rissanen, M., Jokinen, T., Schobesberger, S., Kangasluoma, J., Kontkanen, J., Nieminen, T., Kurtén, T., Nielsen, L. B., Jø rgensen, S., Kjaergaard, H. G., Canagaratna, M., Maso, M. D., Berndt, T., Petäjä, T., Wahner, A., Kerminen, V.-M., Kulmala, M., Worsnop, D. R., Wildt, J., and Mentel, T. F.: A large source of low-volatility secondary organic aerosol., Nature, 506, 476–9, doi:10.1038/nature13032, http://www.ncbi.nlm.nih.gov/pubmed/24572423, 2014.

Gao, W., Shaw, R. H., and Paw, K. T.: Observation of organized structure in turbulent flow within and above a forest canopy, Boundary-Layer Meteorology, 47, 349–377, 1989.

Gu, L., Shugart, H. H., Fuentes, J. D., Black, T. A., and Shewchuk, S. R.: Micrometeorology, biophysical exchanges and NEE decomposition in a two-storey boreal forest - development and test of an integrated model, Agricultural and Forest Meteorology, 94, 123–148, 1999.

Guenther, A., Karl, T., Harley, P., Wiedinmyer, C., Palmer, P. I., and Geron, C.: Estimates of global terrestrial isoprene emissions using MEGAN (Model of Emissions of Gases and Aerosols from Nature), Atmospheric Chemistry and Physics Discussions, 6, 107–173, doi:10.5194/acpd-6-107-2006, http://www.atmos-chem-phys-discuss.net/6/107/2006/, 2006.

Guenther, A. B., Nicholas, C., Fall, R., Klinger, L., Mckay, W. A., and Scholes, B.: A global model of natural volatile organic compound emissions, Journal of Geophysical Research, 100, 8873–8892, 1995.

Haverd, V., Leuning, R., Griffith, D., Gorsel, E., and Cuntz, M.: The turbulent Lagrangian time scale in forest canopies constrained by fluxes, concentrations and source distributions, Boundary-Layer Meteorology, 130, 209–228, doi:10.1007/s10546-008-9344-4, http://www.springerlink.com/index/10.1007/s10546-008-9344-4, 2009.

Helliker, B. R. and Richter, S. L.: Subtropical to boreal convergence of tree-leaf temperatures, Nature, 454, 511–4, doi:10.1038/nature07031, http://www.ncbi.nlm.nih.gov/pubmed/18548005, 2008.

Hourdin, F.: Etude et simulation numérique de la circulation générale des atmosphères planétaires, Ph.D. thesis, 1992.

Hunter, J. D.: Matplotlib: A 2D graphics environment, Computing In Science & Engineering, 9, 90–95, 2007.

Jiménez, C., Prigent, C., Mueller, B., Seneviratne, S. I., McCabe, M. F., Wood, E. F., Rossow, W. B., Balsamo, G., Betts, A. K., Dirmeyer, P. A., Fisher, J. B., Jung, M., Kanamitsu, M., Reichle, R. H., Reichstein, M., Rodell, M., Sheffield, J., Tu, K., and Wang, K.: Global intercomparison of 12 land surface heat flux estimates,

Journal of Geophysical Research, 116, D02 102, doi:10.1029/2010JD014545, http://doi.wiley.com/10.1029/2010JD014545, 2011.

Krinner, G., Viovy, N., de Noblet-Ducoudré, N., Ogee, J., Polcher, J., Friedlingstein, P., Ciais, P., Sitch, S., and Prentice, I. C.: A dynamic global vegetation model for studies of the coupled atmosphere-biosphere system, Global Biogeochemical Cycles, 19, 1–33, doi:10.1029/2003GB002199, 2005.

Lovell, J., Haverd, V., Jupp, D., and Newnham, G.: The Canopy Semi-analytic Pgap And Radiative Transfer (CanSPART) model: Validation using ground based lidar, Agricultural and Forest Meteorology, 158-159, 1–12, doi:10.1016/j.agrformet.2012.01.020, http://linkinghub.elsevier.com/retrieve/pii/S0168192312000512, 2012.

LSCE/IPSL: ORCHIDEE documentation (as at forge.ipsl.jussieu.fr/orchidee/wiki/Documentation), 2012.

Makar, P. A., Fuentes, J. D., Wang, D., Staebler, R. M., and Wiebe, H. A.: Chemical processing of biogenic hydrocarbons within and above a temperate deciduous forest, Journal of Geophysical Research, 104, 3581–3603, doi:10.1029/1998JD100065, http://www.agu.org/pubs/crossref/1999/1998JD100065.shtml, 1999.

Massman, W. J. and Weil, J. C.: An analytical one-dimensional second-order closure model of turbulence statistics and the lagrangian time scale within and above plant canopies of arbitrary structure, Boundary-Layer Meteorology, 91, 81–107, 1999.

McGrath, M. J., Pinty, B., Ryder, J., Otto, J., and Luyssaert, S.: A multilevel canopy radiative transfer scheme based on a domain-averaged structure factor, in prep.

McNaughton, K. G. and van den Hurk, B. J. J. M.: A 'Lagrangian' revision of the resistors in the two-layer model for calculating the energy budget of a plant canopy, Boundary-Layer Meteorology, 74, 261–288, 1995.

Medlyn, B. E., Duursma, R. A., Eamus, D., Ellsworth, D. S., Prentice, I. C., Barton, C. V. M., Crous, K. Y., De Angelis, P., Freeman, M., and Wingate, L.: Reconciling the optimal and empirical approaches to modelling stomatal conductance, Global Change Biology, 17, 2134–2144, doi:10.1111/j.1365-2486.2010.02375.x, http://doi.wiley.com/10.1111/j.1365-2486.2010.02375.x, 2011.

Monteith, J. and Unsworth, M. H.: Principles of Environmental Physics, Elsevier, 2008.

Naudts, K., Ryder, J., J. McGrath, M., Otto, J., Chen, Y., Valade, a., Bellasen, V., Berhongaray, G., Bönisch, G., Campioli, M., Ghattas, J., De Groote, T., Haverd, V., Kattge, J., MacBean, N., Maignan, F., Merilä, P., Penuelas, J., Peylin, P., Pinty, B., Pretzsch, H., Schulze, E. D., Solyga, D., Vuichard, N., Yan, Y., and Luyssaert, S.: A vertically discretised canopy description for ORCHIDEE (SVN r2290) and the modifications to the energy, water and carbon fluxes, Geoscientific Model Development Discussions, 7, 8565–8647, doi:10.5194/gmdd-7-8565-2014, 2014.

Nemitz, E. G., Sutton, M. A., Wyers, G. P., and Jongejan, P. A. C.: Gas-particle interactions above a Dutch heathland: I. Surface exchange fluxes of NH3, SO2, HNO3 and HCl, Atmospheric Chemistry and Physics, 4, 989–1005, 2004a.

Nemitz, E. G., Sutton, M. A., Wyers, G. P., Otjes, R. P., Mennen, M. G., Putten, E. M. V., and Gallagher, M. W.: Gas-particle interactions above a Dutch heathland: II. Concentrations and surface exchange fluxes of atmospheric particles, Atmospheric Chemistry and Physics, 4, 1007–1024, 2004b.

Nobel, P. S.: Physiochemical and environmental plant physiology, Elsevier, 3 edn., 0-12-520026-9, 2005.

Ogée, J., Brunet, Y., Loustau, D., Berbigier, P., and Delzon, S.: MuSICA, a CO2, water and energy multilayer, multileaf pine forest model: evaluation from hourly to yearly time scales and sensitivity analysis, Global Change Biology, 9, 697–717, doi:10.1046/j.1365-2486.2003.00628.x, http://doi.wiley.com/10.1046/j.1365-2486.2003.00628.x, 2003.

Ozflux: Description of Tumbarumba monitoring station (as at www.ozflux.org.au/monitoringsites/tumbarumba), www.ozflux.org.au/monitoringsites/tumbarumba, 2013.

Park, G.-H., Gao, X., and Sorooshian, S.: Estimation of surface longwave radiation components from ground-based historical net radiation and weather data, Journal of Geophysical Research, 113, D04 207, doi:10.1029/2007JD008903, http://doi.wiley.com/10.1029/2007JD008903, 2008.

Penman, H. L. and Schofield, R. K.: Some physical aspects of assimilation and transpiration, Symp. Soc. Exp. Biol., 5, 115–129, 1951.

Pinty, B., Lavergne, T., Dickinson, R. E., Widlowski, J.-L., Gobron, N., and Verstraete, M. M.: Simplifying the interaction of land surfaces with radiation for relating remote sensing products to climate models, Journal of Geophysical Research, 111, 1–20, doi:10.1029/2005JD005952, http://www.agu.org/pubs/crossref/2006/2005JD005952.shtml, 2006.

Pitman, A. J., de Noblet-Ducoudré, N., Cruz, F. T., Davin, E. L., Bonan, G. B., Brovkin, V., Claussen, M., Delire, C., Ganzeveld, L., Gayler, V., van den Hurk, B. J. J. M., Lawrence, P. J., van der Molen, M. K., Müller, C., Reick, C. H., Seneviratne, S. I., Strengers, B. J., and Voldoire, A.: Uncertainties in climate responses to past land cover change: First results from the LUCID intercomparison study, Geophysical Research Letters, 36, L14 814, doi:10.1029/2009GL039076, http://www.agu.org/pubs/crossref/2009/2009GL039076.shtml, 2009.

Polcher, J., McAvaney, B., Viterbo, P., Gaertner, M., Hahmann, A., Mahfouf, J.-F., Noilhan, J., Phillips, T., Pitman, A. J., Schlosser, C., Schulz, J.-P., Timbal, B., Verseghy, D. L., and Xue, Y.: A proposal for a general interface between land surface schemes and general circulation models, Global and Planetary Change, 19, 261–276, http://www.sciencedirect.com/science/article/pii/S0921818198000526, 1998.

Press, W. H.: Numerical recipes in Fortran 77: Second edition, Cambridge University Press, 1992.

Raupach, M. R.: Applying Lagrangian fluid mechanics to infer scalar source distributions from concentration profiles in plant canopies, Agricultural and Forest Meteorology, 47, 85–108, 1989a.

Raupach, M. R.: A practical Lagrangian method for relating scalar concentrations to source distributions in vegetation canopies, Quarterly Journal of the Royal Meteorological Society, 115, 609–632, doi:10.1256/smsqj.48709, http://www.ingentaselect.com/rpsv/cgi-bin/cgi?ini=xref&body=linker&reqdoi=10.1256/smsqj.48709, 1989b.

Richtmyer, R. D. and Morton, K. W.: Difference Methods for Initial-Value Problems (second edition), Wiley-Interscience, 1967.

Saux-Picart, S., Ottlé, C., Perrier, a., Decharme, B., Coudert, B., Zribi, M., Boulain, N., Cappelaere, B., and Ramier, D.: SEtHyS_Savannah: A multiple source land surface model applied to Sahelian landscapes, Agricultural and Forest Meteorology, 149, 1421–1432, doi:10.1016/j.agrformet.2009.03.013, http://linkinghub.elsevier.com/retrieve/pii/S0168192309000847, 2009.

Scheffers, B. R., Phillips, B. L., Laurance, W. F., Sodhi, N. S., Diesmos, A., Williams, E., and Williams, S. E.: Increasing arboreality with altitude: a novel biogeographic dimension, Proceedings of the The Royal Society B, 280, 1–9, doi:10.1098/rspb.2013.1581, 2013.

Schlosser, C. A. and Gao, X.: Assessing Evapotranspiration Estimates from the Second Global Soil Wetness Project (GSWP-2) Simulations, Journal of Hydrometeorology, 11, 880–897, doi:10.1175/2010JHM1203.1, http://journals.ametsoc.org/doi/abs/10.1175/2010JHM1203.1, 2010.

Schulz, J.-P., Dümenil, L., and Polcher, J.: On the Land Surface–Atmosphere Coupling and Its Impact in a Single-Column Atmospheric Model, Journal of Applied Meteorology, 40, 642–663, doi:10.1175/1520-0450(2001)040<0642:OTLSAC>2.0.CO;2, http://journals.ametsoc.org/doi/abs/10.1175/1520-0450(2001)040<0642:OTLSAC>2.0.CO;2, 2001.

Seneviratne, S. I., Corti, T., Davin, E. L., Hirschi, M., Jaeger, E. B., Lehner, I., Orlowsky, B., and Teuling, A. J.: Investigating soil moisture–climate interactions in a changing climate: A review, Earth-Science Reviews, 99, 125–161, doi:10.1016/j.earscirev.2010.02.004, http://linkinghub.elsevier.com/retrieve/pii/S0012825210000139, 2010.

Shuttleworth, W. J. and Wallace, J. S.: Evaporation from sparse crops - an energy combination theory, Quarterly Journal of the Royal Meteorological Society, 111, 839–855, doi:10.1256/smsqj.46909, http://www.ingentaselect.com/rpsv/cgi-bin/cgi?ini=xref&body=linker&reqdoi=10.1256/smsqj.46909, 1985.

Singles, R., Sutton, M., and Weston, K.: A multi-layer model to describe the atmospheric transport and deposition of ammonia in Great Britain, Atmospheric Environment, 32, 393–399, doi:10.1016/S1352-2310(97)83467-X, http://linkinghub.elsevier.com/retrieve/pii/S135223109783467X, 1998.

Sinoquet, H., Le Roux, X., Adam, B., Ameglio, T., and Daudet, F. A.: RATP: a model for simulating the spatial distribution of radiation absorption, transpiration and photosynthesis within canopies: application to an isolated tree crown, Plant, Cell and Environment, 24, 395–406, doi:10.1046/j.1365-3040.2001.00694.x, http://doi.wiley.com/10.1046/j.1365-3040.2001.00694.x, 2001.

Stroud, C., Makar, P. A., Karl, T., Guenther, A. B., Geron, C., Turnipseed, A., Nemitz, E. G., Baker, B., Potosnak, M. J., and Fuentes, J. D.: Role of canopy-scale photochemistry in modifying biogenic-atmosphere exchange of reactive terpene species: Results from the CELTIC field study, Journal of Geophysical Research, 110, 1–14, doi:10.1029/2005JD005775, http://www.agu.org/pubs/crossref/2005/2005JD005775.shtml, 2005.

Verhoef, A. and Allen, S. J.: A SVAT scheme describing energy and CO2 fluxes for multi-component vegetation: calibration and test for a Sahelian savannah, Ecological Modelling, 127, 245–267, doi:10.1016/S0304-3800(99)00213-6, http://linkinghub.elsevier.com/retrieve/pii/S0304380099002136, 2000.

Vieno, M.: The use of an atmospheric chemistry-transport model (FRAME) over the UK and the development of its numerical and physical schemes, Ph.D. thesis, University of Edinburgh, 2006.

Vuichard, N. and Papale, D.: Filling the gaps in meteorological continuous data measured at FLUXNET sites with ERA-interim reanalysis, Earth System Science Data Discussions, 8, 23–55, doi:10.5194/essdd-8-23-2015, www.earth-syst-sci-data-discuss.net/8/23/2015/, 2015.

Waggoner, P. E., Furnival, G. M., and Reifsnyder, W. E.: Simulation of the microclimate in a forest, Forest Science, 15, 37–45, 1969.

Walton, S., Gallagher, M. W., and Duyzer, J. H.: Use of a detailed model to study the exchange of NOx and O3 above and below a deciduous canopy, Atmospheric Environment, 31, 2915–2931, doi:10.1016/S1352-2310(97)00126-X, http://linkinghub.elsevier.com/retrieve/pii/S135223109700126X, 1997.

Wohlfahrt, G. and Cernusca, A.: Momentum transfer by a mountain meadow canopy: a simulation analysis based on Massman's (1997) model, Boundary-Layer Meteorology, 103, 391–407, 2002.

Wolfe, G. M. and Thornton, J. A.: The Chemistry of Atmosphere-Forest Exchange (CAFE) Model – Part 1: Model description and characterization, Atmospheric Chemistry and Physics, 11, 77–101, doi:10.5194/acp-11-77-2011, http://www.atmos-chem-phys.net/11/77/2011/http://www.atmos-chem-phys-discuss.net/10/21721/2010/, 2010.

Yamazaki, T., Kondo, J., and Watanabe, T.: A heat-balance model with a canopy of one or two layers and its application to field experiments, Journal of Applied Meteorology, 31, 86–103, 1992.

Zhao, W. and Qualls, R. J.: A multiple-layer canopy scattering model to simulate shortwave radiation distribution within a homogeneous plant canopy, Water Resources Research, 41, 1–16, doi:10.1029/2005WR004016, http://doi.wiley.com/10.1029/2005WR004016, 2005.

Zhao, W. and Qualls, R. J.: Modeling of long-wave and net radiation energy distribution within a homogeneous plant canopy via multiple scattering processes, Water Resources Research, 42, 1–13, doi:10.1029/2005WR004581, http://doi.wiley.com/10.1029/2005WR004581, 2006.

List of Figures

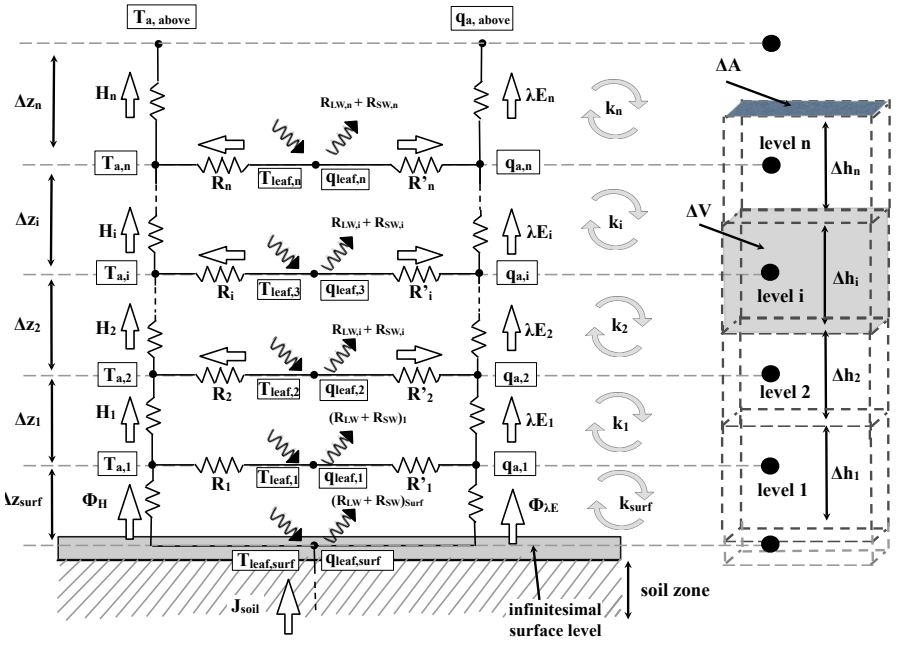

Figure 1. Resistance analogue for a multilayer canopy approximation of n levels, to which the energy balance applies at each level. Refer to Table 1 for interpretation of the symbols.

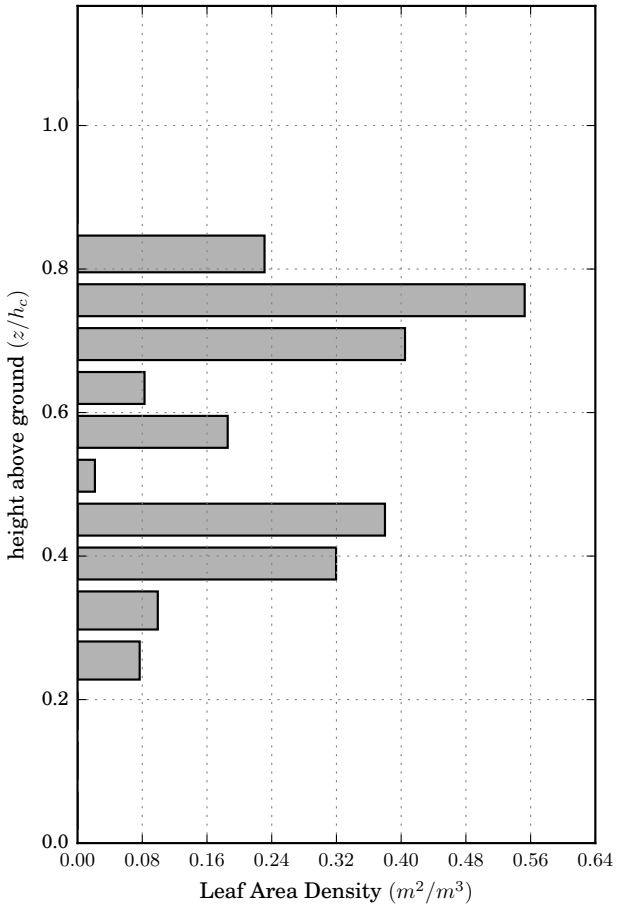

Figure 2. Simulated Leaf Area Density Profile corresponding to the forest canopy at the Tumbarumba site used in this study.

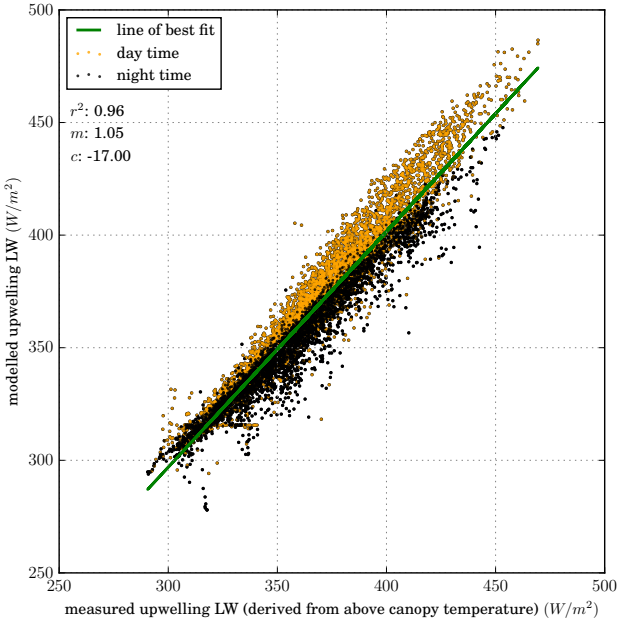

Figure 3. Correlation of observed upwelling longwave radiation (derived from the measured above-canopy temperature) and the upwelling longwave radiation that is simulated by ORCHIDEE-CAN. Nighttime data (corresponding to a downwelling shortwave radiation of < 10 Wm^{-2}) are plotted in black, and daytime data are plotted in orange.

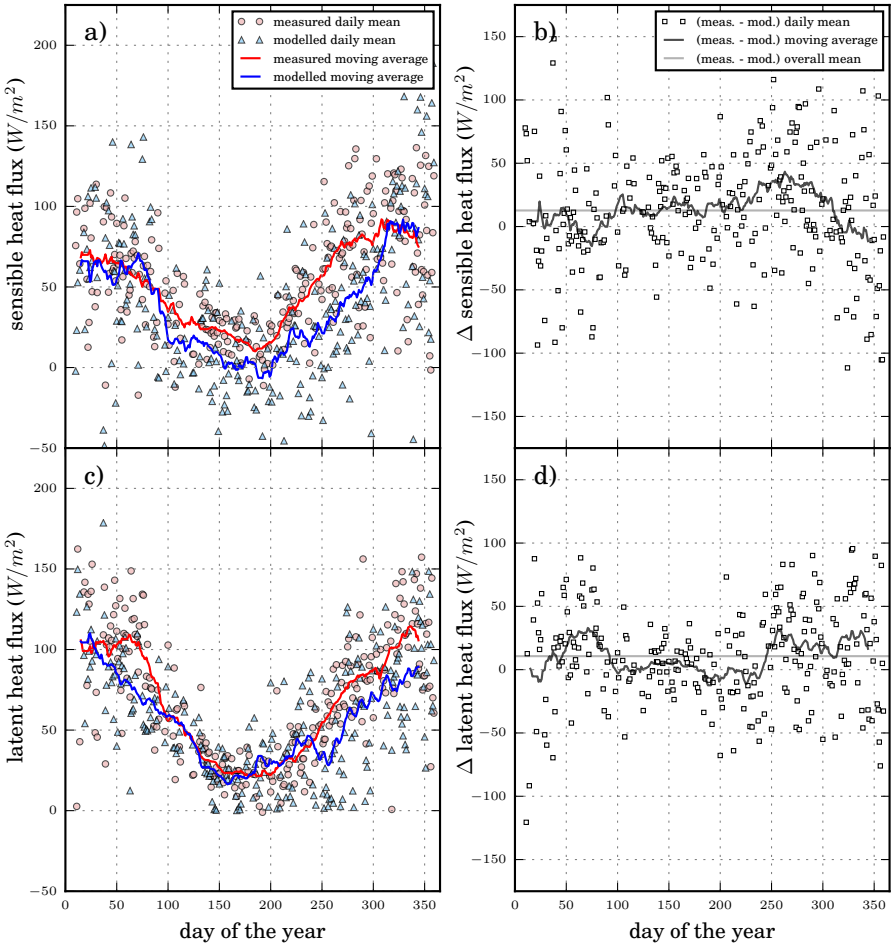

Figure 4. Daily mean for measured (circles) and modelled (triangles) over a year-long run for (a) sensible heat flux; (b) difference between measured and modelled sensible heat flux; (c) latent heat flux; and (d) difference between measured and modelled latent heat flux. One in every 5 data points is shown, for clarity. Thick lines show the respective 20 day moving average respectively for each dataset. Graphs (b) and (d) also show the overall mean of individual data points.

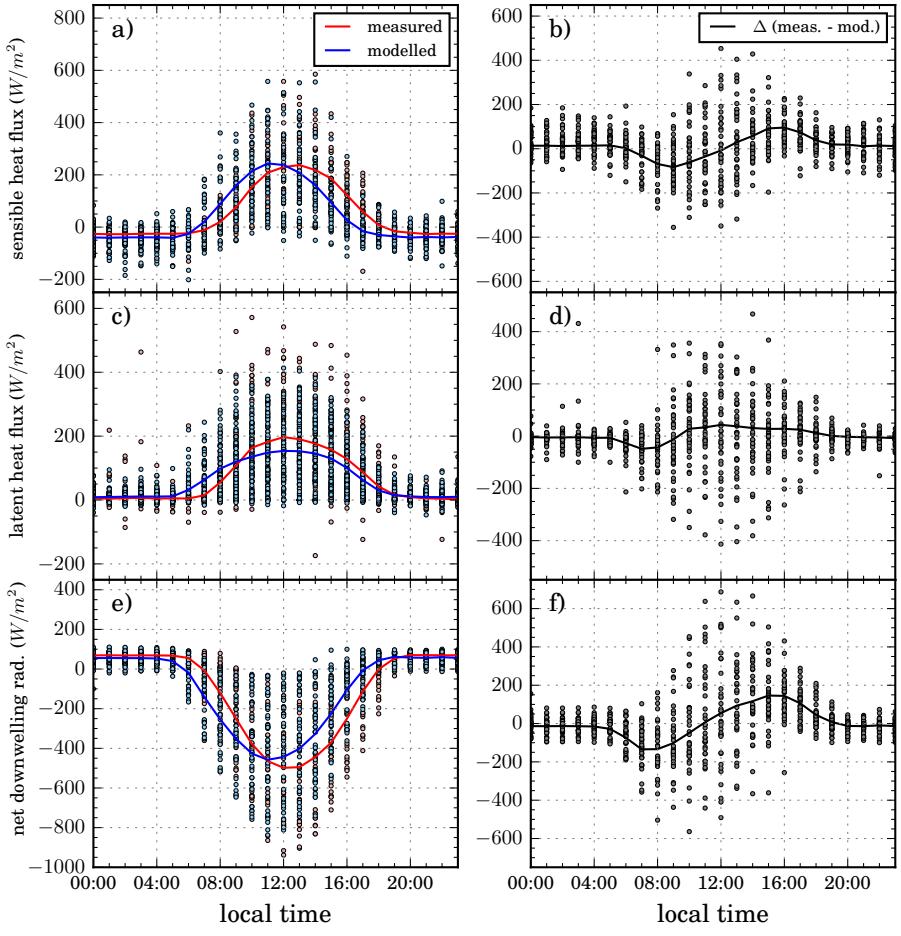

Figure 5. Hourly means for measured (circles) and modelled (triangles) for (a) sensible heat flux; (b) difference between measured and modelled sensible heat flux, as calculated over the period of 2006. One in every 10th day is plotted for clarity; (c) and (d): as above for latent heat flux; (e) and (f): as above for net radiation. Continuous lines show the overall mean.

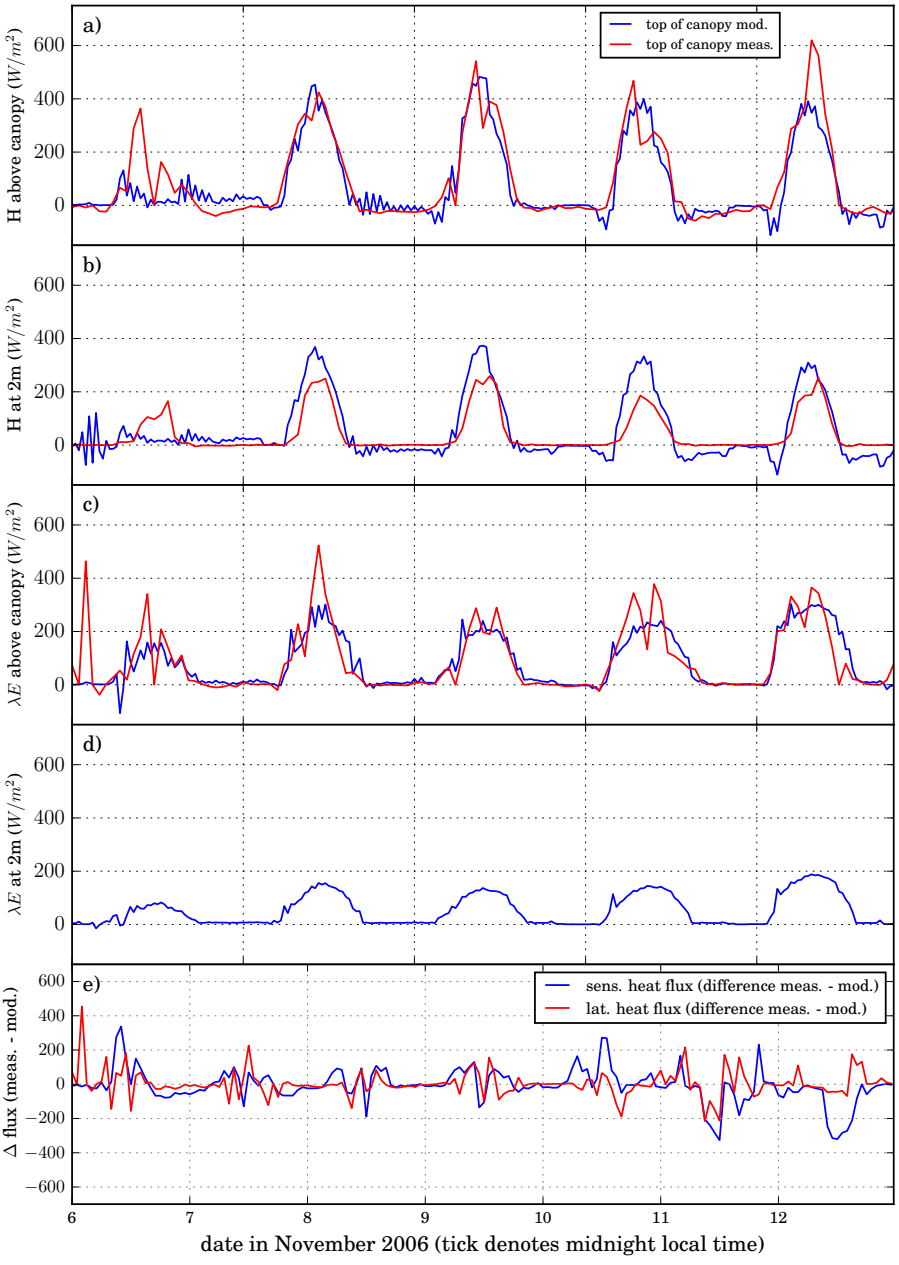

Figure 6. Short term simulated and observed energy fluxes: (a) sensible heat fluxes at a height of 50m; (b) as (a) for latent heat flux; (c) measured and modelled sensible heat flux at 2m above the ground; (d) modelled latent heat flux at 2m above the ground (measurements not available); (e) difference in measured and modelled sensible and latent heat flux at a height of 50m

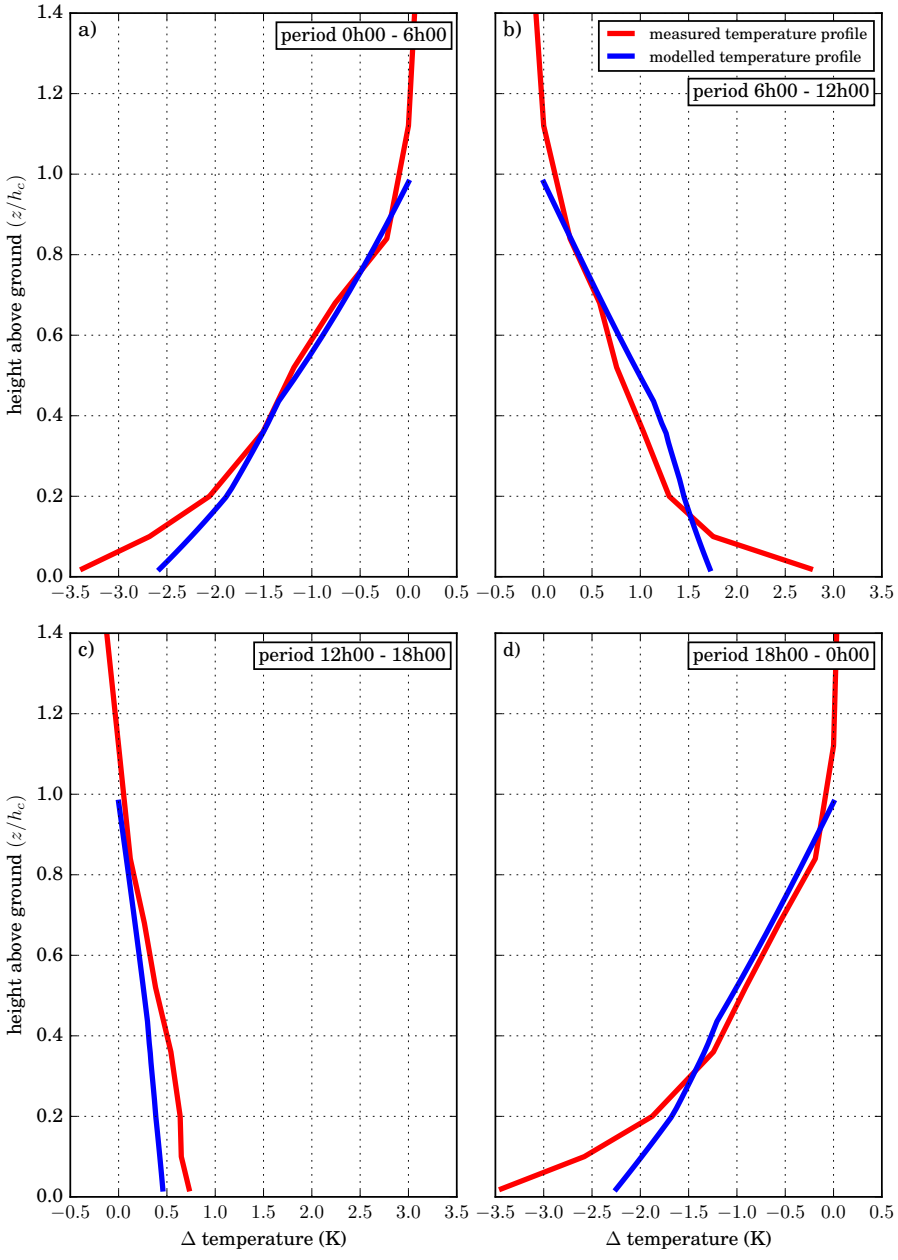

Figure 7. Vertical within canopy temperature profiles for four six-hour periods corresponding to the same time period as in Figure 6. Mean modelled temperature profiles (bold in blue) within the canopy against the measured temperature profiles (bold in red) for the time periods: (a) 0h00-6h00; (b) 6h00-12h00; (c) 12h00-18h00 and (d) 18h00-0h00, both expressed as a difference from the temperature at the top of canopy.

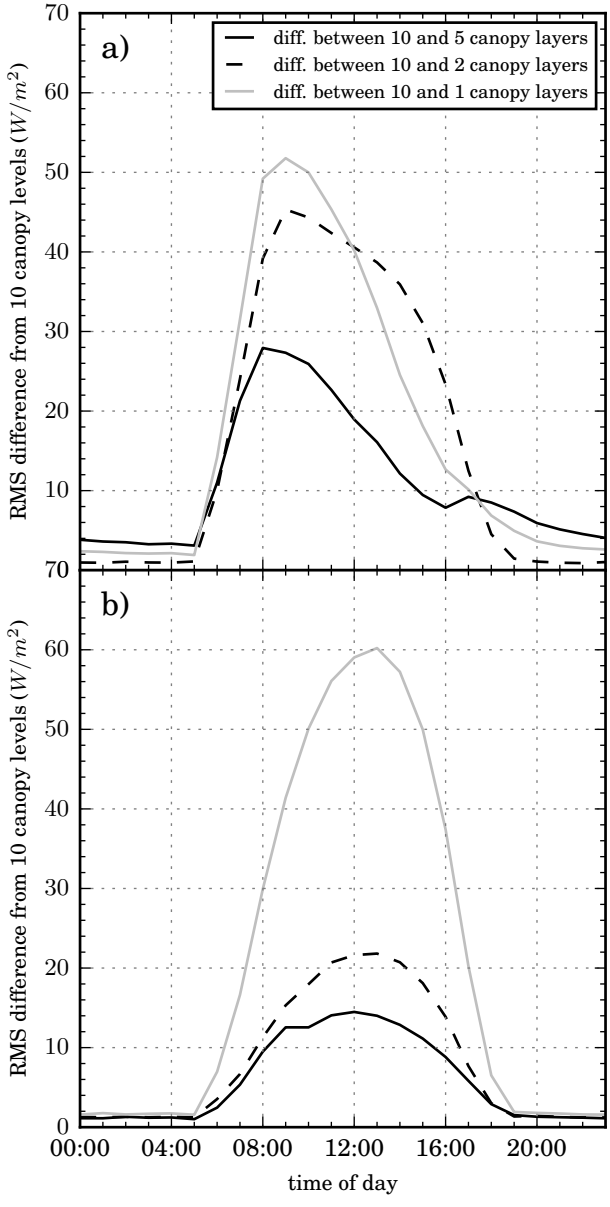

Figure 8. Comparison of model performance for a set-up with 10 canopy layers (out of 30 total profile levels), 5 canopy layers (of 15 total profile levels), 2 canopy levels (of 8 total profile levels) and 1 canopy levels (of 5 total profile levels), expressed as an hourly average for a year-long run (a) Root mean square difference between the different model runs for sensible heat flux; (b) as (a) for latent heat flux

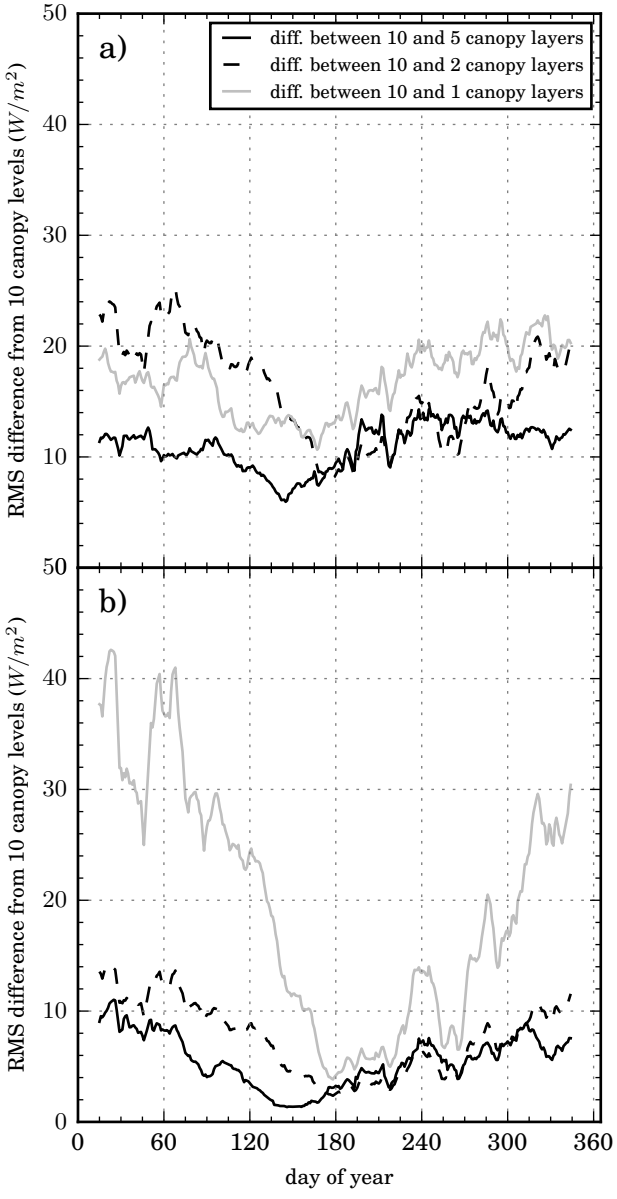

Figure 9. As for Figure 8 for a set-up with 10 canopy layers (out of 30 total profile levels), 5 canopy layers (of 15 total profile levels), 2 canopy levels (of 8 total profile levels) and 1 canopy levels (of 5 total profile levels), for a run over the course of a year, expressed as a daily average (a) 20 day moving average of the root mean square difference of the daily mean of sensible heat flux; (b) as (a) for latent heat flux

List of Tables

Table 1. Symbolic notation used throughout the manuscript (Latin)

symbol	description
$A_{q,i}, B_{q,i}, C_{q,i}, D_{q,i}$	Components for substituted equation ii)
$A_{T,i}, B_{T,i}, C_{T,i}, D_{T,i}$	Components for substituted equation i)
C_p^{air}	Specific heat capacity of air $(J/(kgK))$
$D_{h,air}$	heat diffusivity of air (cm^2/s)
D_{h,H_2O}	heat diffusivity of water vapour (cm^2/s)
d_l	characteristic leaf length (m)
E_i, F_i, G_i	Components for substituted equation iii)
$G_{leaf}(\mu)$	Leaf orientation function
$H_i, \lambda E_i$	Sensible and latent heat flux at level i, respectively (W/m^2)
$H_{tot}, \lambda E_{tot}$	Total sensible heat and latent heat flux at canopy top, respectively (W/m^2)
$\Im(\ell)$	effect of canopy structure on the passage of LW radiation
J_{soil}	Heat flux from the sub-soil (W/m^2)
k_i	Diffusivity coefficient for level i (m^2/s)
k_i^*	Modified diffusivity coefficient for level i (m^2/s)
k_{surf}	Diffusivity coefficient for the surface level (m^2/s)
ℓ_i	cumulative Leaf Area Index, working up to level i (m^2/m^2)
Nu	Nusselt number $(-)$
Pr	Prandtl number $(-)$
$R_{b,i}, R'_{b,i}$	Boundary layer resistance at level i for heat and water vapour, respectively (s/m)
$R_{s,i}$	Stomatal resistance at level i (s/m)
R_i, R'_i	Total flux resistances at level i for sensible and latent heat flux, respectively (s/m)
$R_{LW,i}, R_{SW,i}$	Long-wave and short wave radiation received by level i, respectively (W/m^2)
R_{nf}	Lagrangian near field correction factor $(-)$
Re	Reynold's number $(-)$
q_i^a	Atmospheric specific humidity at level i (kg/kg)
$q_{leaf,i}$	Leaf specific humidity at level i (kg/kg)
$q_{sat}^{T_{leaf}}$	Saturated specific humidity of leaf at level at i (kg/kg)
q^t	Specific humidity (kg/kg)
Sh	Sherwood number $(-)$
T_i^a	Atmospheric temperature at level i (K)
T_L	Lagrangian timescale (s)
$T_{leaf,i}$	Leaf temperature at level i (K)
T^t, T^{t+1}	Temperature at the 'present' and 'next' timestep respectively (K)

Table 1 (continued). Symbolic notation used throughout the manuscript (Greek)

symbol	description
$\alpha_{i,j}^{LW}$	an element of the LW radiation transfer matrix (-)
α_i	abbreviation in the leaf vapour pressure assumption
β_i	abbreviation in the leaf vapour pressure assumption
ΔA_i	Difference in area of vegetation level i (m^2)
Δh_i	Thickness of level i (m)
ΔV_i	Difference in volume of vegetation level i (m^3)
Δz_i	Difference in height between potential at level i and level $i+1$ (m)
$\Delta \aleph_{surf}$	LW radiation that is absorbed at level i (W/m^2)
$\Delta \aleph_i$	LW radiation that is absorbed at level i (W/m^2)
$\Delta \aleph_{above}$	LW radiation that is absorbed above the canopy (W/m^2)
ϵ_i	Emissivity fraction at level i $(-)$
θ_i	Leaf layer heat capacity at level i $(J/(kgK))$
μ	Kinematic viscosity of air (cm^2/s)
ρ_v, ρ_a	Vegetation and atmospheric density, respectively (kg/m^3)
η_1	Non-implicit part of LW radiation transfer matrix component $(-)$
η_2	Implicit part part of LW radiation component $(-)$
η_3	Multilevel albedo derived SW radiation component $(-)$
θ_0	Heat capacity of the infinitesimal surface layer $(J/(Km^2))$
λ	Latent heat of vapourisation (J/kg)
ξ_1, ξ_2, ξ_3, ξ_4	Abbreviations for surface boundary layer conditions
σ	Stefan-Boltzmann constant (5.67 x 10^{-8} $Wm^{-2}K^{-4}$)
σ_w	Standard deviation in vertical velocity (m/s)
τ	Lagrangian emission lifetime (s)
$\phi_H^{t+1}, \phi_{\lambda E}^{t+1}$	Respectively sensible and latent heat flux from the infinitesimal surface layer (W/m^2)
ψ_i^{abs}	absorbed albedo component at level i (fraction)
ψ_i^{in}	fraction of 'incoming' transmitted, back- or forward- SW radiation $(fraction)$
ψ_i^{out}	fraction of 'outgoing' transmitted, back- or forward- SW radiation $(fraction)$
Ω_1, Ω_2... Ω_8	Abbreviations for surface boundary layer conditions
ω_i	Leaf interception coefficient at level i $(-)$

Table 2. Input coefficients at the top layer of the model, where $A_{T,n}, B_{T,n}$... etc are the respective coefficients at the top of the surface model and $A_{T,atmos}$, $B_{T,atmos}$ are the coefficients at the lowest level of the atmospheric model

stand-alone model	**coupled model**
$A_{T,n} = 0$	$A_{T,n} = A_{T,atmos}$
$B_{T,n} = B_{T,input}$	$B_{T,n} = B_{T,atmos}$
$C_{T,n} = 0$	$C_{T,n} = 0$
$D_{T,n} = 0$	$D_{T,n} = 0$
$A_{q,n} = 0$	$A_{q,n} = A_{q,atmos}$
$B_{q,n} = B_{q,input}$	$B_{q,n} = B_{q,atmos}$
$C_{q,n} = 0$	$C_{q,n} = 0$
$D_{q,n} = 0$	$D_{q,n} = 0$

Table 3. Tuning coefficients used in the model for simulation described in this work

symbol (as here)	**description**	**code ref.**	**initial value**	**tuned value(s)**	**reference example**
$R_{b,fac}$	tuning coeff. for $R_{b,i}$	br_fac	1.0	0.857	-
$R_{g,fac}$	tuning coeff. for R_g	sr_fac	1.0	2.426	-
number of levels	number of levels	nlvls	30	15, 8, 5	-
R_{nf}	eddy diff. tuning coef.	k_eddy_fac	1.0	0.4	Makar et al. (1999)
m_{veg}	leaf mass	(leaf_tks·rho_veg)	$0.21 kg/m^2$	$0.14 kg/m^2$	Nobel (2005), section 7.1
$G_{leaf}(\mu)$	leaf orientation coeff.	bigk_lw	1.0	0.75	Gu et al. (1999)
a_3, a_4, a_5	coefficients for C_{Deff}	a_3	0.452	0.360	Wohlfahrt and Cernusca (2002)
		a_4	1.876	-0.081	
		a_5	0.065	0.028	